NATIONAL ADVISORY COMMITTEE
FOR AERONAUTICS

TECHNICAL NOTE 2229

THE EFFECT OF END PLATES ON SWEPT WINGS AT LOW SPEED

By John M. Riebe and James M. Watson

Langley Aeronautical Laboratory
Langley Air Force Base, Va.

Washington
November 1950

NATIONAL ADVISORY COMMITTEE FOR AERONAUTICS

TECHNICAL NOTE 2229

THE EFFECT OF END PLATES ON SWEPT WINGS AT LOW SPEED

By John M. Riebe and James M. Watson

SUMMARY

An investigation was made in the Langley 300 MPH 7- by 10-foot
tunnel to determine the effects of various sizes and shapes of end plates
on the aileron characteristics and on the aerodynamic characteristics in
pitch and yaw of a wing of aspect ratio 2 with no taper and a sweepback
of 45° and of a wing of aspect ratio 4, taper ratio 0.6, and sweepback
of 46.7°. Free-roll characteristics were obtained with two end-plate
configurations on a wing of aspect ratio 3, taper ratio 0.6, and a
sweepback of 35° in order to determine the effect of end plates on wing
damping in roll.

The addition of the end plates to the swept wings increased the
lift-curve slope, reduced the maximum lift-drag ratio, generally
decreased the maximum lift coefficient, and increased the longitudinal
stability slightly in the low lift coefficient range.

The variation of wing effective dihedral with lift coefficient was
reduced by increase in end-plate size. The effective dihedral at zero
lift could be changed from positive to negative by lowering the end
plates. The directional stability of the swept wings was increased with
increase in end-plate area and with rearward movement of the end plates.

The flap-type aileron and spoiler-aileron effectiveness increased
with the addition of end plates to the swept wings; however, the increase
of the wing damping in roll may reduce the rolling effectiveness for some
end-plate configurations. In addition, end plates located below the wing
chord line reduced the adverse yaw of flap-type ailerons.

INTRODUCTION

Theoretical and experimental investigations on unswept wings and
tail surfaces (for example, references 1 to 3) have indicated that the
addition of end plates will generally improve the wing aerodynamic
efficiency. The use of end plates which acted as a barrier to the span-
wise flow along the outboard portion of the span and around the tips of
airfoils resulted in increased lift-curve slopes, less induced drag,
and higher maximum lift coefficients.

The application of end plates to sweptback wings has been considered as a possible means of overcoming some of the lateral-stability diffi- culties (such as large changes in effective dihedral with lift coefficient) and other adverse effects (such as reduced lift-curve slope, maximum lift, and aileron effectiveness) that result through the use of sweepback in wings.

The present paper presents the results of a low-speed investigation made in the Langley 300 MPH 7- by 10-foot tunnel to determine the effects of end plates having various sizes and shapes on the stability and con- trol characteristics of several swept wings. For the most part, the results are for end plates on a wing of aspect ratio 2 with no taper and a sweepback of 45° with limited results for two other swept wings of aspect ratios 3 and 4.

The results, in general, include the longitudinal stability, lateral stability, and lateral control characteristics as affected by end-plate size, shape, and location. The lateral control characteristics include results for both flap and spoiler ailerons, and results of a free-roll investigation of two end-plate configurations on a wing of aspect ratio 3, taper ratio 0.6, and 35° sweepback to determine the effect of end plates on wing damping in roll.

SYMBOLS

The forces and moments measured on the wings (fig. 1) are presented about the stability axes, which intersect at the center-of-moment posi- tions shown in figures 2, 6, and 9. The Z-axis is in the plane of symmetry and perpendicular to the relative wind, the X-axis is in the plane of symmetry and perpendicular to the Z-axis, and the Y-axis is mutually perpendicular to the X-axis and Z-axis (fig. 1).

The symbols used are as follows:

C_L lift coefficient (L/qS)

C_D drag coefficient (D/qS)

C_Y lateral-force coefficient (Y/qS)

C_l rolling-moment coefficient (L'/qSb)

C_m pitching-moment coefficient (M'/qSb)

C_n yawing-moment coefficient (N/qSb)

L   lift of model, pounds   (-Z)

D   drag of model, pounds   (-X   when $\psi = 0°$)

Y   force along Y-axis, pounds

X   force along X-axis, pounds

Z   force along Z-axis, pounds

L'   rolling moment about X-axis, foot-pounds

M'   pitching moment about Y-axis, foot-pounds

N   yawing moment about Z-axis, foot-pounds

L/D   lift-drag ratio

q   free-stream dynamic pressure, pounds per square
             foot $\left(\frac{1}{2}\rho V^2\right)$

p   rate of roll, radians per second

S   wing area (6.00 square feet on wing model of aspect
             ratio 2, 3.17 square feet on wing model of aspect
             ratio 3, and 2.25 square feet on wing model of aspect
             ratio 4)

S_e lateral area of both end plates, square feet

$\bar{c}$ wing mean aerodynamic chord (1.73 feet on wing model
             of aspect ratio 2, 1.05 feet on wing model of aspect
             ratio 3, and 0.765 foot on wing model of aspect
             ratio 4)

c   wing tip chord

b   wing span (3.46 feet on wing model of aspect ratio 2,
             3.09 feet on wing model of aspect ratio 3, and 3.00 feet
             on wing model of aspect ratio 4)

h'   effective height of end plate $(S_e/2c)$, feet

V   air velocity, feet per second

ρ mass density of air, slugs per cubic foot

α angle of attack of chord line at root of model, degrees

ψ angle of yaw, degrees

δ_a aileron deflection, measured in a plane perpendicular to the hinge axis, degrees

Δ increment in coefficient due to end plates

M   Mach number (V/a)

R   Reynolds number $(\rho V \bar{c}/\mu)$

a   speed of sound, feet per second

μ coefficient of absolute viscosity, slugs per foot-second

A   wing aspect ratio $\left(b^2/S\right)$

A'   effective wing aspect ratio with end plates

λ taper ratio   (Tip chord/Root chord)

Λ sweep angle of quarter-chord line

$pb/2V$ wing-tip helix angle, radians

C_{l_p} coefficient of damping in roll $\left(\dfrac{\partial C_l}{\partial\left(\frac{pb}{2V}\right)}\right)$

$$C_{L_\alpha} = \frac{\partial C_L}{\partial\alpha}$$

$$C_{l_{\delta_a}} = \frac{\partial C_l}{\partial\delta_a}$$

$$C_{n_{\delta_a}} = \frac{\partial C_n}{\partial\delta_a}$$

$$\left(\frac{pb}{2V}\right)_{\delta_a} = \frac{\partial\left(\frac{pb}{2V}\right)}{\partial\delta_a}$$

$$C_{l_\psi} = \frac{\partial C_l}{\partial \psi}$$

$$C_{Y_\psi} = \frac{\partial C_Y}{\partial \psi}$$

$$C_{n_\psi} = \frac{\partial C_n}{\partial \psi}$$

Subscript:

max   maximum

CORRECTIONS

Wing of aspect ratio 2.- The angle-of-attack and the drag data have been corrected for jet-boundary effects according to the methods outlined in reference 4 for unswept wings; as can be seen from reference 5, there is little effect of sweep on the jet-boundary effects. Blockage corrections were applied to the test data by the method of reference 6. The data have been corrected for the effects of the model support strut by the use of tare corrections determined for the wing without end plate.

Wing of aspect ratio 3.- Blockage corrections were applied to the test data by the method of reference 6. A small tare correction because of bearing friction has been applied to the free-roll results in the form of an increment of damping-in-roll coefficient equal to -0.005.

Wing of aspect ratio 4.- The angle-of-attack and the drag data have been corrected for jet-boundary effects according to the methods outlined in reference 4.

MODEL AND APPARATUS

Wing of aspect ratio 2.- The 45° sweptback wing model of aspect ratio 2 (fig. 2) was mounted horizontally on a single strut in the Langley 300 MPH 7- by 10-foot tunnel (fig. 3). The untapered wing had NACA 64A010 airfoil sections normal to the wing leading edge and had neither twist nor dihedral. The wing, which was constructed of wood, had rounded tips which were removed forward of the aileron hinge line for the investigation with end plates.

The end plates investigated were constructed of $\frac{1}{8}$-inch sheet duralumin with rounded edges to the dimensions shown in figure 4. A cutout was made in the trailing edge of each end plate to allow for deflection of the outboard, half-semispan, 0.25-chord, plain, sealed aileron.

The stepped spoiler ailerons investigated were constructed of $\frac{1}{8}$-inch aluminum angles which were fastened to the wing upper surface as shown in figure 5 and projected 8 percent of the wing chord. This configuration corresponded to one of the more promising stepped-spoiler configurations for this wing plan form (unpublished data).

Wing of aspect ratio 3.- The 35° sweptback wing model of aspect ratio 3 and taper ratio 0.6 used for the free-roll investigation is shown in figure 6. The wing was supported by a sting extending forward into the test section from a vertical strut. A schematic drawing of the support system and rolling apparatus is shown in figure 7. The angle of attack of the model was changed by varying the angle of incidence of the wing relative to the sting. Rolling-moment data were obtained by an electrical strain gage with the sting restrained in roll. When the model was permitted to roll freely under the moment created by the deflected aileron, the rate of roll was recorded electrically.

The ordinates of the symmetrical, 12-percent-thick airfoil section of the 35° sweptback wing are given in table I. The model was constructed of steel and the two end plates were constructed of $\frac{1}{8}$-inch aluminum sheet with rounded edges. The model was equipped with an outboard flap-type aileron with sealed gap.

Wing of aspect ratio 4.- The 46.7° sweptback wing of aspect ratio 4 and taper ratio 0.6 was tested on a sting-mounted electrical strain-gage balance (fig. 8). The sting was attached to a single strut which varied the angle of attack and angle of yaw of the model. The wing remained in the center of the test section at various angles of yaw but was displaced vertically at various angles of attack.

Dimensions of the wing, which had NACA 65A006 airfoil sections, and of the end plates investigated on this wing are given in figures 9 and 10, respectively. The end plates were constructed of $\frac{1}{8}$-inch or $\frac{1}{16}$-inch duralumin with rounded or beveled edges.

TESTS

The conditions and types of tests made on the three wings in the Langley 300 MPH 7- by 10-foot tunnel are as follows:

Condition or type of test	Wing		
	Aspect ratio 2	Aspect ratio 3	Aspect ratio 4
q	100	145	110
M	0.27	0.32	0.28
R	3.2×10^6	2.3×10^6	1.84×10^6
Longitudinal stability	$\alpha = -6^\circ$ to stall	------------------------------	$\alpha = -6^\circ$ to 24°
Lateral stability	$\begin{cases} \psi = 5^\circ \text{ and } -5^\circ \\ \alpha = -6^\circ \text{ to stall} \end{cases}$	------------------------------	$\psi = 0^\circ \text{ and } 5^\circ$ $\alpha = -4^\circ$ to stall
Directional stability	$\begin{cases} \psi = 5^\circ \text{ and } -5^\circ \\ \alpha = -6^\circ \text{ to stall} \end{cases}$	------------------------------	------------------------
Lateral control Flap-type ailerons Spoiler ailerons	$\alpha = -6^\circ$ to stall $\delta_a = -10^\circ, 0^\circ, 5^\circ, \text{ and } 10^\circ$ -0.08 wing chord projection	$\alpha = 6.5^\circ$ $\delta_a = -15^\circ$ to 9.4° ------------------	------------------ ------------------
Free roll	------------------------------	$\begin{cases} \alpha = 0.3^\circ, 3.5^\circ, \text{ and } 6.5^\circ \\ \delta_a = -15^\circ \text{ to } 9.4^\circ \end{cases}$	------------------

RESULTS

The results are presented in the following figures:

The slopes presented in the figures were taken over a lift-coefficient
range of about ±0.1, an angle-of-attack range of ±2°, an aileron-
deflection range of ±10° or 0° to 10°, and a yaw range of 0° to 5°.
(For the wing of aspect ratio 4, the values of ΔC_{L_α} (presented in
fig. 15) were determined from lateral-stability tests made through an
angle-of-attack range at 5° angle of yaw; however, a few tests made at
0° angle of yaw showed that small angles of yaw had little effect on
the incremental values of C_{L_α}.)

DISCUSSION

Aerodynamic Characteristics in Pitch

Lift-curve slope.- The addition of end plates to either the wing
of aspect ratio 2 or aspect ratio 4 increased the lift-curve slope in
the low lift-coefficient range (figs. 11 and 15). A comparison of the
increase in lift-curve slope for the sweptback wings with end plates

obtained from the experimental data of this investigation and that
obtained from unswept-wing end-plate theory (reference 7) with the use
of reference 8 shows good agreement (fig. 15). It can be seen that
the increments in C_{L_α} due to end plates decrease as the wing aspect
ratio is increased for a given value of h'/b but are relatively inde-
pendent of end-plate shape. This is as would be expected, since the
theory of reference 7 indicates that regardless of wing aspect ratio
the increase in A'/A is dependent on end-plate-height - wing-span
ratio and equal increases in A'/A result in smaller increases in C_{L_α}
at the higher aspect ratios (reference 8).

The increases in lift-curve slope (fig. 15) represent increases in
effective aspect ratios of about 1.8 for the wing of aspect ratio 2 and
3.6 for the wing of aspect ratio 4 at values of $\frac{h'}{b} = 0.5$.

A comparison of the results of this investigation of swept wings
with the results of unswept wings (reference 3) indicates similar changes
in ΔC_{L_α} and A'/A with h'/b for values of h'/b less than 0.5; for
values greater than 0.5, however, the unswept-wing data indicate that
the changes in ΔC_{L_α} and A'/A are less than those predicted by the
theory of reference 7. It would be expected, therefore, that further
increases in end-plate size on swept wings would give further increases
in C_{L_α}, but that the increases would probably be less than those pre-
dicted from the theory of reference 7. Wing taper ratio might be
expected to have an effect on ΔC_{L_α} for a given value of h'/b for
wings having fairly high taper. The results of this investigation
indicate that the effects of taper, if any, are very small for the range
of model geometry used.

The results of this investigation indicate that the lift-curve
slope of a swept wing with end plate can be satisfactorily predicted
from the theory for end plates on unswept wings up to a value of h'/b
of 0.5.

Maximum lift coefficient.- The maximum lift coefficient $C_{L_{max}}$
was generally decreased by the addition of end plates to the 45° swept-
back wing of aspect ratio 2 (figs. 11 and 16). This decrease is opposite
to the effect found on unswept wings (fig. 16) where increases in $C_{L_{max}}$
generally resulted from installation of end plates.

End plates located below the wing chord plane were found to have
less adverse effect on the values of $C_{L_{max}}$ than the same end plates
located above the chord plane. In fact, three of the end plates tested
below the chord plane (a triangular end plate, a semicircular end plate,

and a 45° sweptback end plate, all extending $c/2$ below the chord plane) had a negligible effect on $C_{L_{max}}$.

Drag coefficient.- The drag coefficients of the 45° sweptback wing of aspect ratio 2 were generally increased by the addition of the various end plates to the wing, except in the intermediate lift-coefficient range of about 0.4 to 0.8 where the reduction in induced drag resulting from the increase in wing effective aspect ratio exceeded the drag of the end plates (fig. 11). Comparing the incremental drag coefficients estimated for unswept wings by the method of reference 1 with the experimental values for the swept wings of aspect ratios 2 and 4 (fig. 17) shows very similar trends. For the calculations, a skin-friction drag coefficient of 0.011 was assumed for the end plates. The estimations show that very little, if any, drag reduction can be expected below lift coefficients of about 0.4. The comparison is limited to lift coefficients up to about 0.6 since the lift curves (fig. 11) indicated a nonlinear variation of lift coefficient with angle of attack at higher values of C_L. Above values of $C_L = 0.8$ the data, in general, show increases in drag coefficient when the end plate is added to the wing.

Tuft studies of some of the end plates of the present investigation showed that there was unsteady flow on the surface of the end plate. This unsteady flow developed at intermediate angles of attack and gradually became more unsteady as the angle of attack was increased. The disturbed flow was generally more prevalent on the outboard surfaces of the end plate. It is believed that more careful design of the airfoil section of the end plate could result in more favorable drag characteristics at the higher lift coefficients.

The reduction in drag coefficient was less for the swept wing of aspect ratio 4 than for the swept wing of aspect ratio 2 (fig. 17). These results are consistent with the trend indicated in reference 1 and correspond to the previously noted condition wherein larger increments of lift-curve slope were obtained on the wing of aspect ratio 2 than on the wing of aspect ratio 4 with the addition of end plates of a given area ratio. (See fig. 15.)

The change in the values of $(L/D)_{max}$ for the wing of aspect ratio 2 generally had some scatter with end-plate size and shape (fig. 18); however, the values of $(L/D)_{max}$ generally decreased with increases in end-plate area ratio. Inspection of figure 11 shows that $(L/D)_{max}$ occurs at lift coefficients less than about 0.3. The results (fig. 17) indicate that unless the end-plate drag is very small no appreciable gains in $(L/D)_{max}$ can be expected since there is an increase in drag coefficients due to the end plate for lift coefficients below 0.4.

Longitudinal stability.- The addition of end plates to the swept-back wing of aspect ratio 2 resulted in an increase in the longitudinal stability of the wing in the 0.1 to 0.65 lift-coefficient range (fig. 11). The shift in aerodynamic center varied almost linearly with end-plate area, the aerodynamic center moving back about 5 percent mean aerodynamic chord as the end plate was increased to $\frac{S_e}{S}$ = 1. Variations in end-plate shape and location had only small effects on the longitudinal stability. The increase in longitudinal stability of the sweptback wing probably is due to a shift of the center of pressure outboard as a result of restraint of flow about the wing tip with the end plate in place.

Data obtained with the sweptback wing of aspect ratio 4 (not presented herein) showed similar results.

Lateral Stability

Effective dihedral.- The rate of change of effective dihedral with lift coefficient at low lift coefficients $\partial C_{l_\psi}/\partial C_L$ was reduced with increase in end-plate area on both the sweptback wings of aspect ratios 2 and 4 (figs. 12, 19, and 20). The reduction in $\partial C_{l_\psi}/\partial C_L$ was generally independent of end-plate shape. The small end plates located ahead of the tip chord (fig. 20) generally appeared to be more effective in reducing $\partial C_{l_\psi}/\partial C_L$ than end plates located farther back.

The reduction in the values of $\partial C_{l_\psi}/\partial C_L$ with increase in end-plate area can be partly attributed to a side force on the end plates. As the wing angle of attack increases the end plates move downward relative to the moment axis, and the side force acting on these end plates produces a rolling moment opposite to that produced by the wing. If the value of C_{Y_ψ} (fig. 21) obtained in the investigation and the geometric properties of the wing of aspect ratio 2 are used, the computed reduction in $\partial C_{l_\psi}/\partial C_L$ due to the end plates is only about 1/3 the reduction shown in figure 19. The remaining reductions in $\partial C_{l_\psi}/\partial C_L$ may have resulted from the end plates causing separation and loss of lift on the leading wing and reducing the tip losses on the trailing wing.

The value of the wing effective-dihedral parameter C_{l_ψ} at zero lift was dependent upon the end-plate area and upon the distribution of end-plate area above and below the wing-tip chord line (figs. 12, 19, and 20). Positive increments in C_{l_ψ} resulted from placing the end-plate area above the wing chord line and negative increments were obtained when the end-plate area was added below the chord line. This

change in C_{l_ψ} with end-plate position results from the side force of
the end plate (figs. 21 and 22) acting above and below the chord line
and amounted to an increment of C_{l_ψ} of about 0.003 when an end plate
of $\dfrac{S_e}{S} = 0.5$ was placed either above or below the chord line on the
wing of aspect ratio 2.

The maximum effective dihedral C_{l_ψ} was obtained on both the wing of
aspect ratio 2 (fig. 12) and aspect ratio 4 at moderate lift coefficients
and the values of $C_{l_{\psi_{max}}}$ exhibited the same trends with increase in end-
plate area as were exhibited at zero lift (figs. 19 and 20). Unpublished
data indicate that an increase in Reynolds number to values corresponding
to flight would increase the maximum effective dihedral by extending the
range of linear variation of C_{l_ψ} with C_L to higher lift coefficients
and would thus delay and possibly decrease the reversal tendencies
of C_{l_ψ} exhibited by most of the wing and wing-end-plate combinations
at the low Reynolds numbers of the present investigation.

Yawing-moment coefficient.- The plain wings of aspect ratios 2 and 4
had approximately neutral directional stability $\left(C_{n_\psi} \approx 0\right)$ over the
lift-coefficient range (figs. 12 and 21). An increase in directional
stability $\left(C_{n_\psi}\right.$ becoming more negative$\left.\right)$ occurred with increase in end-
plate area; this effect was reasonably independent of end-plate location
above and/or below the wing chord line. This fact is indicated by the
data of figures 21 and 22, which are for a lift coefficient of 0.5 and
also generally applied to the variation of C_{n_ψ} with end-plate area
throughout the lift-coefficient range (fig. 12). The data of figure 21
also show an effect of forward and rearward location of a given end-
plate area on the values of C_{n_ψ}; this effect results from a change in
the moment arm between the wing center-of-moment position and the center
of pressure developed on the end plate at angles of yaw.

Side-force coefficient.- The variation of C_{Y_ψ} with C_L was
negligible throughout the lift-coefficient range for all end-plate con-
figurations on the wing of aspect ratio 2 (fig. 12). Increase in end-
plate size resulted in larger positive changes of C_{Y_ψ} for the swept
wings of both aspect ratios 2 and 4; this effect appeared fairly inde-
pendent of end-plate shape (figs. 21 and 22).

Aileron Characteristics

Flap-type ailerons.- For most of the wing end-plate configurations
on the swept wing of aspect ratio 2 the rolling-moment coefficients
produced by the aileron were largest at low angles of attack (fig. 13).

The aileron-effectiveness parameter $C_{l_{\delta_a}}$ increased when the area of end plates was increased (fig. 23) and $C_{l_{\delta_a}}$ generally became more effective when the end-plate area was concentrated near the wing trailing edge. One of the most promising end plates was the triangular-shaped end plate which had a value of $C_{l_{\delta_a}}$ at 0° angle of attack (0.0013) almost equal to that of the maximum obtained with any of the end plates in the investigation and yet had a relatively small end-plate area (fig. 23).

The wing with end plates having area only above the wing chord line had positive values of $C_{n_{\delta_a}}$, whereas the wing with end plates having area only below the wing chord line had negative values of $C_{n_{\delta_a}}$ (fig. 23). For a given end-plate shape and position, increasing the end-plate area resulted in an increase in the magnitude of the values of $C_{n_{\delta_a}}$. One of the largest positive and one of the largest negative values of $C_{n_{\delta_a}}$ were produced by the wing with the relatively small triangular end plate located above and below the wing chord line, respectively.

Analysis of yawing-moment data obtained from aileron tests made through an angle-of-attack range (but which are not presented herein) has indicated that the reversal in $C_{n_{\delta_a}}$ as the end plate was shifted from above the wing chord line to below the wing chord line resulted primarily from a change in lateral force on the end plate. With end plates located above the wing chord line, down deflections of the right aileron resulted in side force in the negative direction on the right end plate because of the increased negative pressure above the wing. Positive yawing moment on the wing resulted because the center of pressure of the end plate was behind the center of moments of the wing. With an end plate located below the wing chord line, down deflections of the right aileron resulted in negative yawing moment because of the increased positive pressure below the wing and the positive side force. With ailerons located on both wings the effects mentioned above would be additive. For example, with end plates located below the wing chord line, a negative yawing moment would be produced from down deflection of the right aileron and also from up deflection of the left aileron.

Spoiler ailerons.- At angles of attack below approximately 16°, the addition of the circular end plate to the swept wing of aspect ratio 2 increased the spoiler-aileron effectiveness substantially (approximately a 75-percent increase at $\alpha = 0^{\circ}$). (See fig. 14.) The increased effectiveness of the spoiler aileron probably resulted from the increased effective aspect ratio and correspondingly higher lift developed by the wing-end-plate combination. Above 16° angle of attack, where the lift of the wing with end plates was less than that of the plain wing, the

effectiveness of the spoiler aileron on the plain wing was greater than on the wing with end plates (fig. 14).

Above 2^O angle of attack, in the region where the end plates had a favorable effect on C_l, the value of C_n produced by the spoiler ailerons was reduced when the end plates were added to the wing. The yawing moments were unfavorable for the wing with the circular end plates (fig. 14) above an angle of attack of 17°.

Rolling Characteristics

The addition of the end plates to the 45° sweptback wing of aspect ratio 2 resulted in increases in $C_{l_{\delta_a}}$; however, the wing damping-in-roll coefficient C_{l_p} may increase at a greater rate with the addition of the end plates than did $C_{l_{\delta_a}}$ and thus result in lower values of $pb/2V$. In order to investigate this effect, a few static-roll and free-to-roll tests were made on a roll rig (fig. 7) of a 35° sweptback wing of aspect ratio 3 (fig. 6). One of the end-plate configurations tested on the 35° sweptback wing was similar to that tested on the 45° sweptback wing of aspect ratio 2 with which the largest value of $C_{l_{\delta_a}}$ was obtained.

For the other end-plate configuration investigated on this wing, the upper half of the aforementioned end plate was removed. The flap-type aileron on the 35° sweptback wing did not extend to the wing tip; therefore, no cutout was made in the end plate to permit the aileron to deflect - as was necessary on the 45° sweptback wing of aspect ratio 2. The plain-wing data for the 35° sweptback wing presented herein were obtained by extrapolating some unpublished data obtained in the Langley high-speed 7- by 10-foot tunnel at high subsonic Mach numbers. These data obtained at high Mach numbers were readily extrapolated to the Mach number of the present investigation because they varied linearly with Mach number at all except the highest Mach numbers.

Results of the static-roll tests of the 35° sweptback wing at $\alpha = 6.5^O$ with and without the two aforementioned end-plate configurations show some nonlinearity of C_l with aileron deflection for the wing with end plates (fig. 24). The value of $C_{l_{\delta_a}}$ determined from figure 24 resulted in similar aileron-effectiveness trends with end plates as the data obtained on the 45° sweptback wing of aspect ratio 2 over the same deflection range (figs. 13 and 23).

The effect of the two end-plate configurations on the variation of $pb/2V$ with aileron deflection was determined from free-roll tests at angles of attack of 0.3^O, 3.5^O, and 6.5^O. The variation of $pb/2V$

over the aileron-deflection range is linear (fig. 25). The parameter $(pb/2V)_{\delta_a}$ was reduced by the addition of the end plates throughout the angle-of-attack range tested; this reduction in $(pb/2V)_{\delta_a}$ varied little with end-plate area (figs. 25 and 26) for these two end-plate configurations. Although $C_{l_{\delta_a}}$ increased with end-plate area, the damping-in-roll coefficient C_{l_p} increased at about the same rate, as shown by values of C_{l_p} computed from the data of figures 24 to 26, (-0.305 for the plain wing, -0.365 for the wing with the sweptback end plate located below the wing chord line, and -0.436 for the sweptback end plate located above and below the wing chord line). The C_{l_p} values were determined from the relationship

$$C_{l_p} = - \frac{C_l}{pb/2V} = - \frac{C_{l_{\delta_a}}}{(pb/2V)_{\delta_a}}$$

The values of C_{l_p} were computed for an angle of attack of 6.5° inasmuch as no static rolling-moment data were obtained at any other angle of attack. The increase in the values of C_{l_p} was proportional to end-plate area; that is, doubling the end-plate area about doubled the increase in C_{l_p}.

As noted previously, the triangular-shaped end plate of smaller area than end plates of other shapes may be utilized to obtain a given increase in $C_{l_{\delta_a}}$ (fig. 23). Because the damping in roll is shown to vary with end-plate area, the triangular end plate should result in a smaller increment of C_{l_p}. It may therefore be possible for low-aspect-ratio sweptback wings with end plates of this type to have about the same or larger values of $(pb/2V)_{\delta_a}$ as those of plain wings.

Unpublished data from a free-roll investigation made in the Langley 300 MPH 7- by 10-foot tunnel actually did show a very slight increase in $(pb/2V)_{\delta_a}$ when a small end plate was attached to a sweptback-wing model with the end-plate area concentrated near the aileron. The wing receiving benefits from the addition of end plates - such as increased lift-curve slope or reduced variation of effective dihedral with lift coefficient - would thus not be penalized by reduced rolling power.

CONCLUDING REMARKS

An investigation was made in the Langley 300 MPH 7- by 10-foot
tunnel to determine the effects on aileron characteristics and on wing
characteristics in pitch and yaw of various sizes and shapes of end
plates on several sweptback wings.

The addition of end plates to sweptback wings increased the lift-
curve slope in the low-lift-coefficient range. This increase in lift-
curve slope tended to increase with end-plate size and could be pre-
dicted from unswept-wing end-plate theory. The end plates also generally
decreased the maximum lift coefficient, decreased the maximum lift-drag
ratio, and slightly increased the longitudinal stability in the low-
lift-coefficient range.

The variation of wing effective dihedral with lift coefficient was
appreciably reduced by increase in end-plate size. The effective
dihedral at zero lift could be changed from positive to negative by
lowering the end plates. The directional stability of the swept wings
was increased with increase in end-plate area and with rearward move-
ment of the end plates.

Although the end plates increased the flap-type aileron and spoiler-
aileron effectiveness, free-roll tests showed that end plates also
increased the damping in roll and may result in a reduction in rolling
effectiveness for some end-plate configurations. In addition, end plates
located below the wing chord line reduced the adverse yaw of flap-type
ailerons.

Langley Aeronautical Laboratory
        National Advisory Committee for Aeronautics
                Langley Air Force Base, Va., August 24, 1950

REFERENCES

1. Hemke, Paul E.: Drag of Wings with End Plates. NACA Rep. 267, 1927.

2. Mangler, W.: The Lift Distribution of Wings with End Plates. NACA TM 856, 1938.

3. Bates, William R.: Collection and Analysis of Wind-Tunnel Data on the Characteristics of Isolated Tail Surfaces with and without End Plates. NACA TN 1291, 1947.

4. Gillis, Clarence L., Polhamus, Edward C., and Gray, Joseph L., Jr.: Charts for Determining Jet-Boundary Corrections for Complete Models in 7- by 10-Foot Closed Rectangular Wind Tunnels. NACA ARR L5G31, 1945.

5. Polhamus, Edward C.: Jet-Boundary-Induced-Upwash Velocities for Swept Reflection-Plane Models Mounted Vertically in 7- by 10-Foot, Closed, Rectangular Wind Tunnels. NACA TN 1752, 1948.

6. Herriot, John G.: Blockage Corrections for Three-Dimensional-Flow Closed-Throat Wind Tunnels, with Consideration of the Effect of Compressibility. NACA RM A7B28, 1947.

7. Von Kármán, Th., and Burgers, J. M.: General Aerodynamic Theory - Perfect Fluids. Airfoils and Airfoil Systems of Finite Span. Vol. II of Aerodynamic Theory, div. E, ch. IV, sec. 19, W. F. Durand, ed., Julius Springer (Berlin), 1935, pp. 211-212.

8. Polhamus, Edward C.: A Simple Method of Estimating the Subsonic Lift and Damping in Roll of Sweptback Wings. NACA TN 1862, 1949.

TABLE I

AIRFOIL SECTION ORDINATES OF 35° SWEPTBACK WING

[All dimensions in percent of wing chord parallel
to plane of symmetry of wing]

Station	Ordinate
0	0
.587	1.096
.880	1.323
1.466	1.669
2.926	2.260
5.830	2.998
8.710	3.492
11.568	3.863
17.215	4.393
22.773	4.752
28.241	4.995
33.620	5.149
38.912	5.232
44.116	5.220
49.234	5.130
54.265	4.909
59.212	4.551
64.074	4.078
68.959	3.532
73.546	2.955
78.158	2.382
82.688	1.840
87.137	1.338
91.504	.876
95.792	.441
100.000	.021
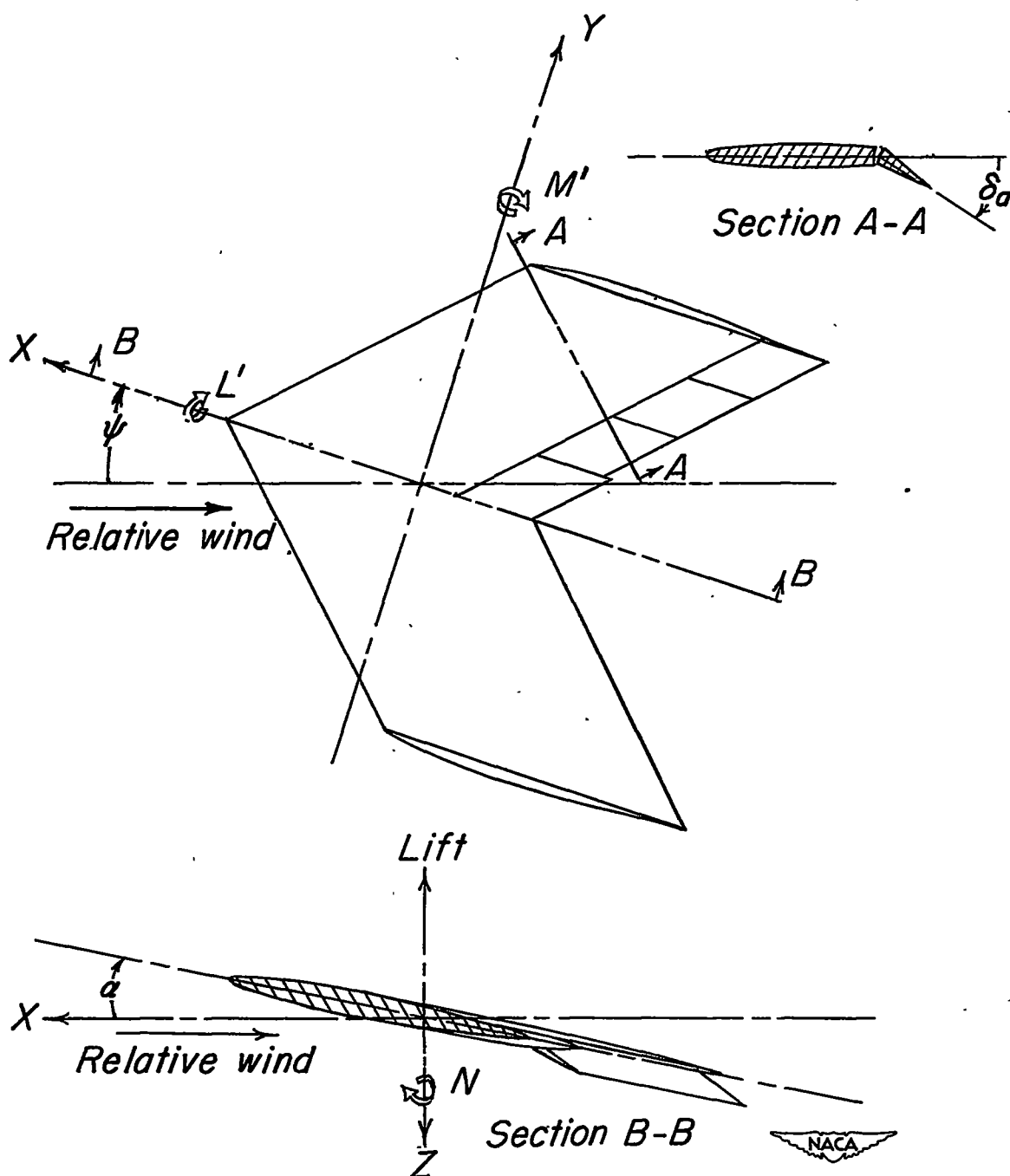
Figure 1.- System of stability axes. Positive values of forces, moments, and angles are indicated by arrows.
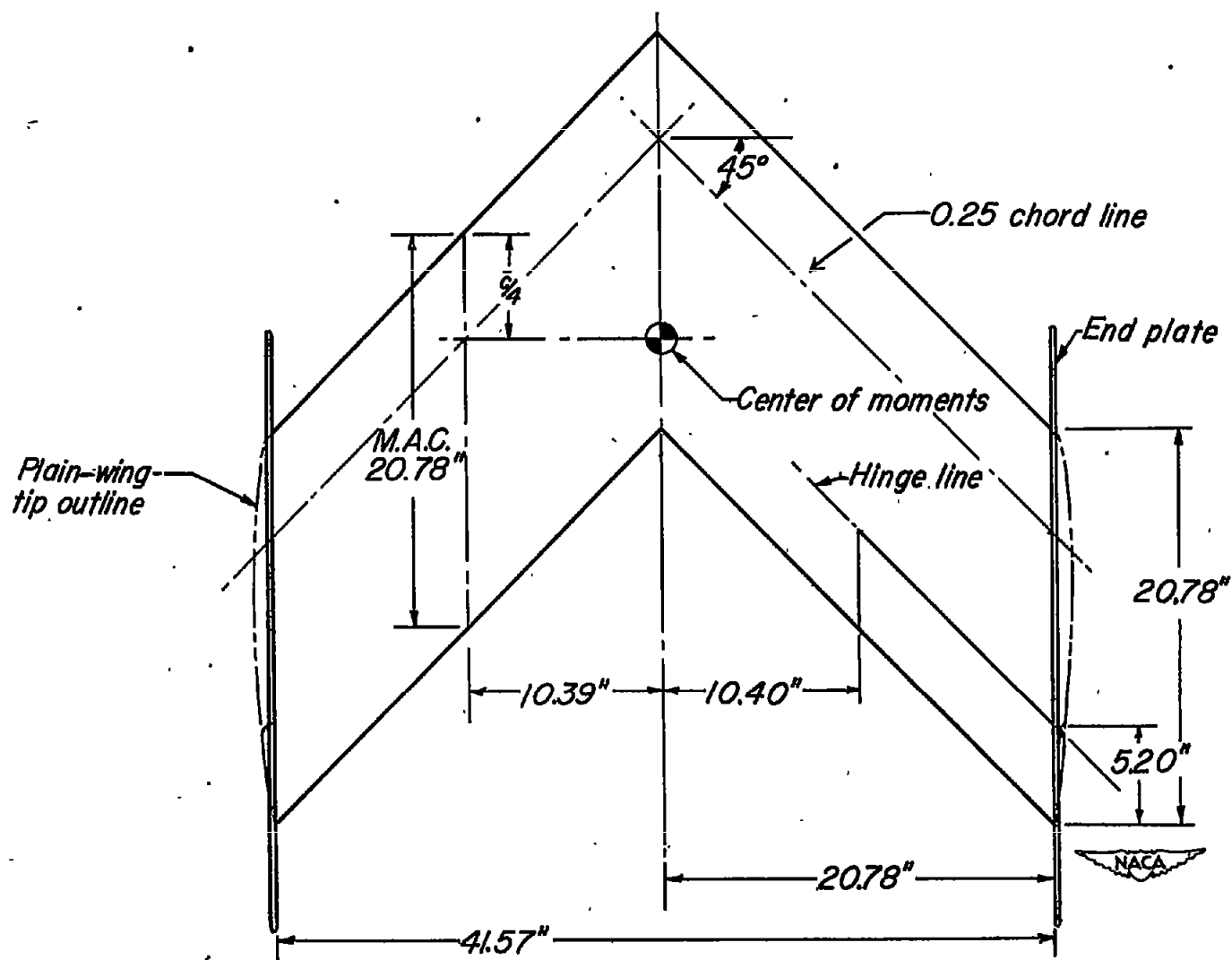
Figure 2.- Geometric characteristics of the 45° sweptback wing of aspect ratio 2 and taper ratio 1 with various end plates. S = 6 square feet.
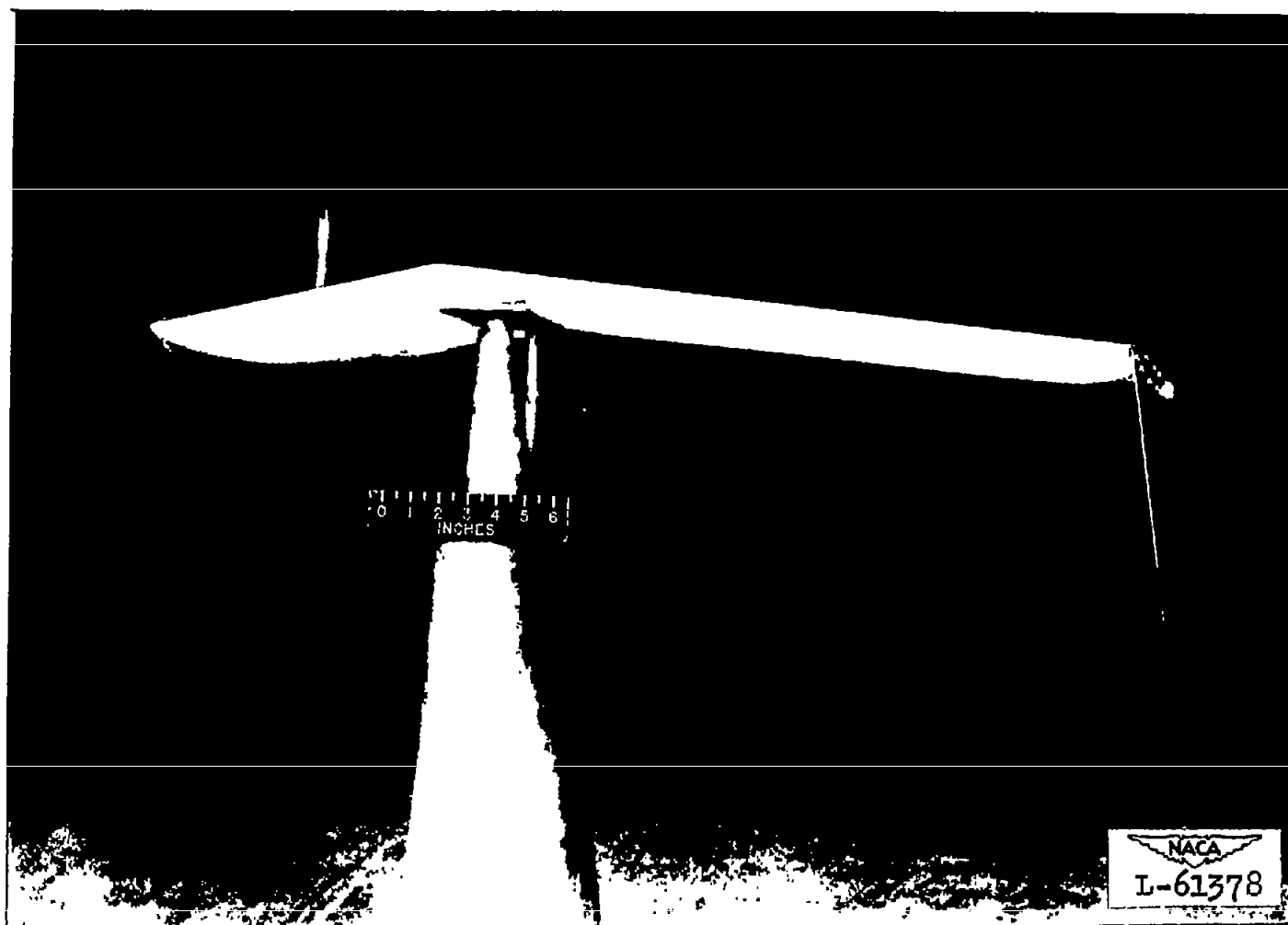
Figure 3.- The 45° sweptback wing of aspect ratio 2 with triangular end
plates mounted on single strut in the Langley 300 MPH 7- by 10-foot
tunnel. $\delta_a = 10°$.
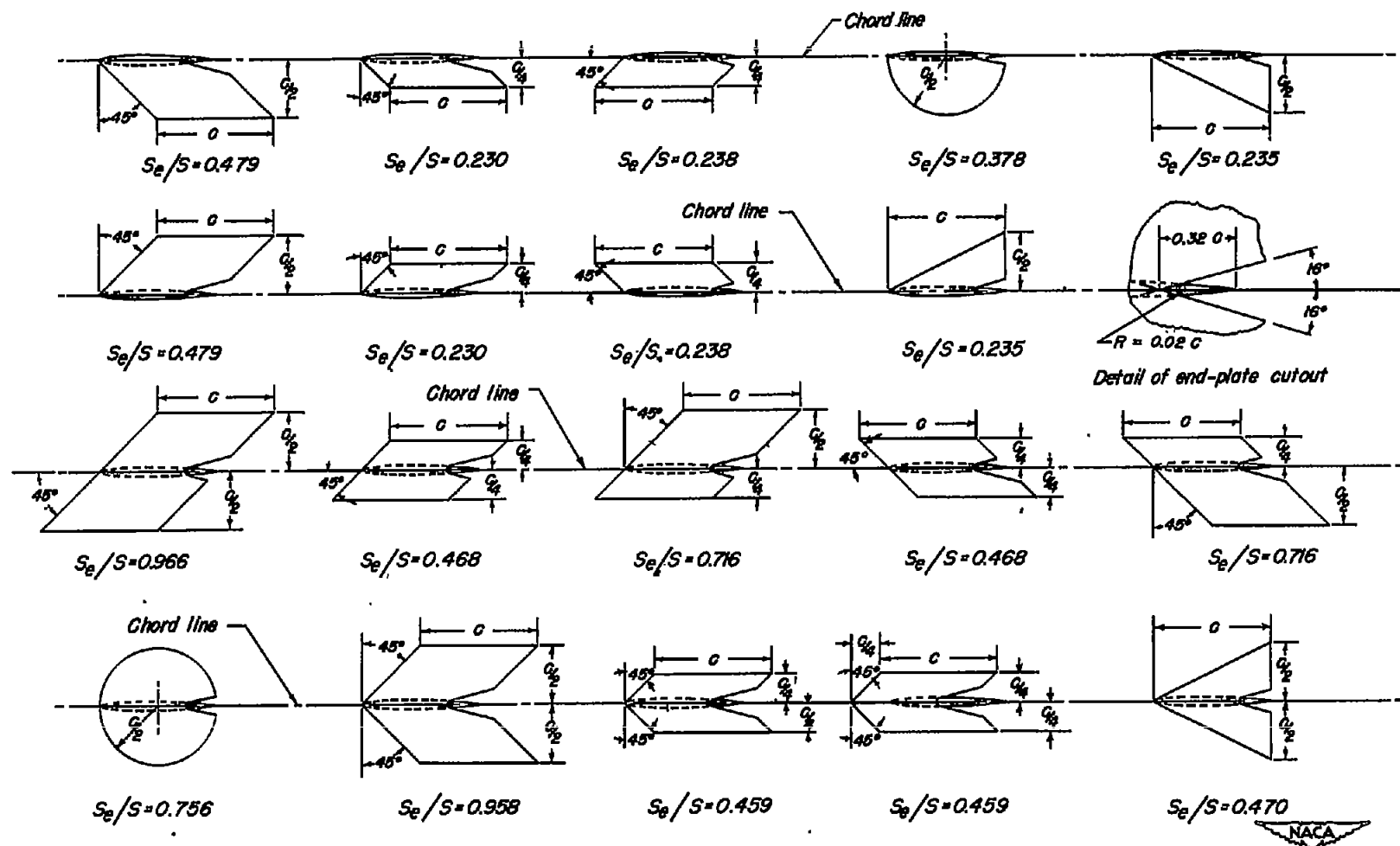
Figure 4.- Geometric characteristics of the various end plates investigated on the 45° sweptback wing of aspect ratio 2.
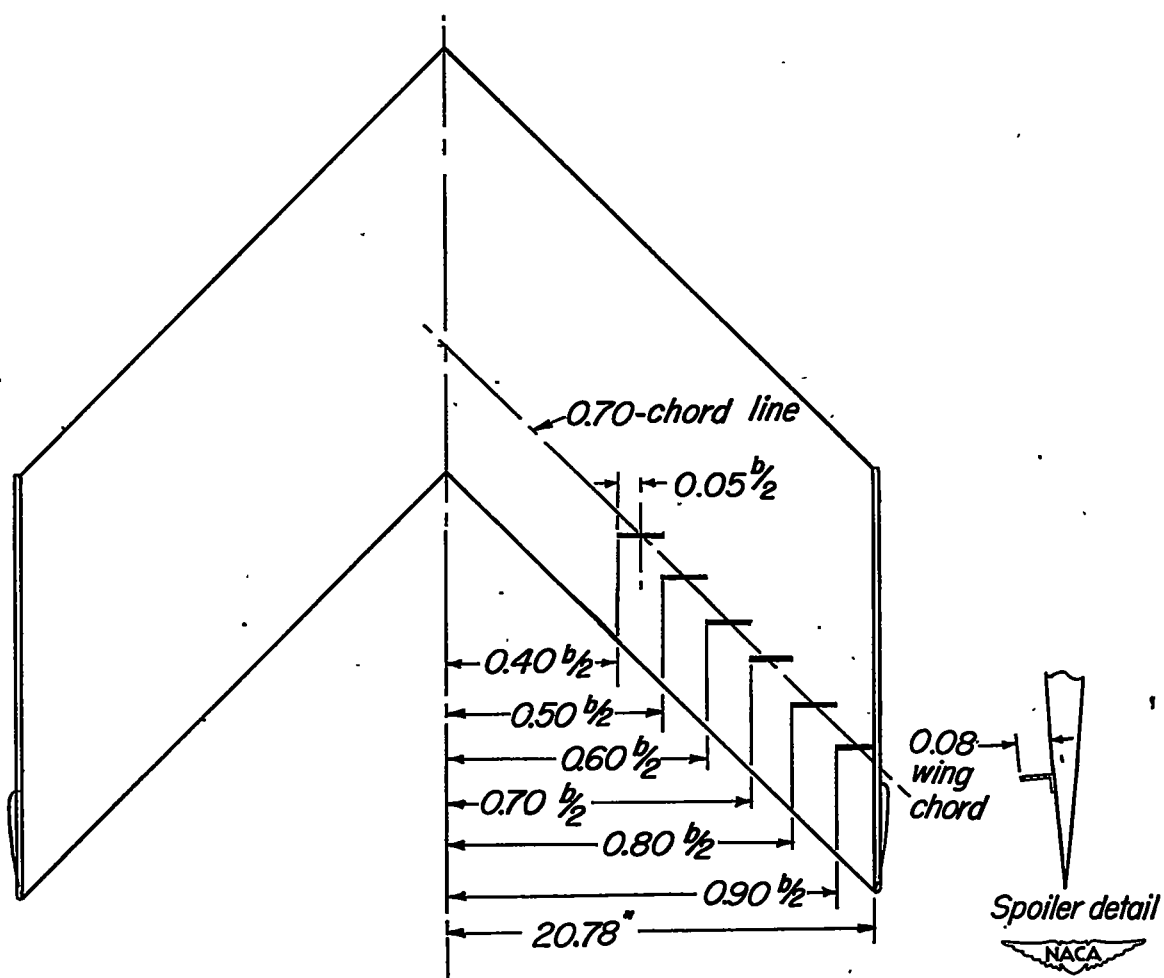
Figure 5.- Stepped spoiler ailerons investigated on the 45° sweptback wing
of aspect ratio 2.
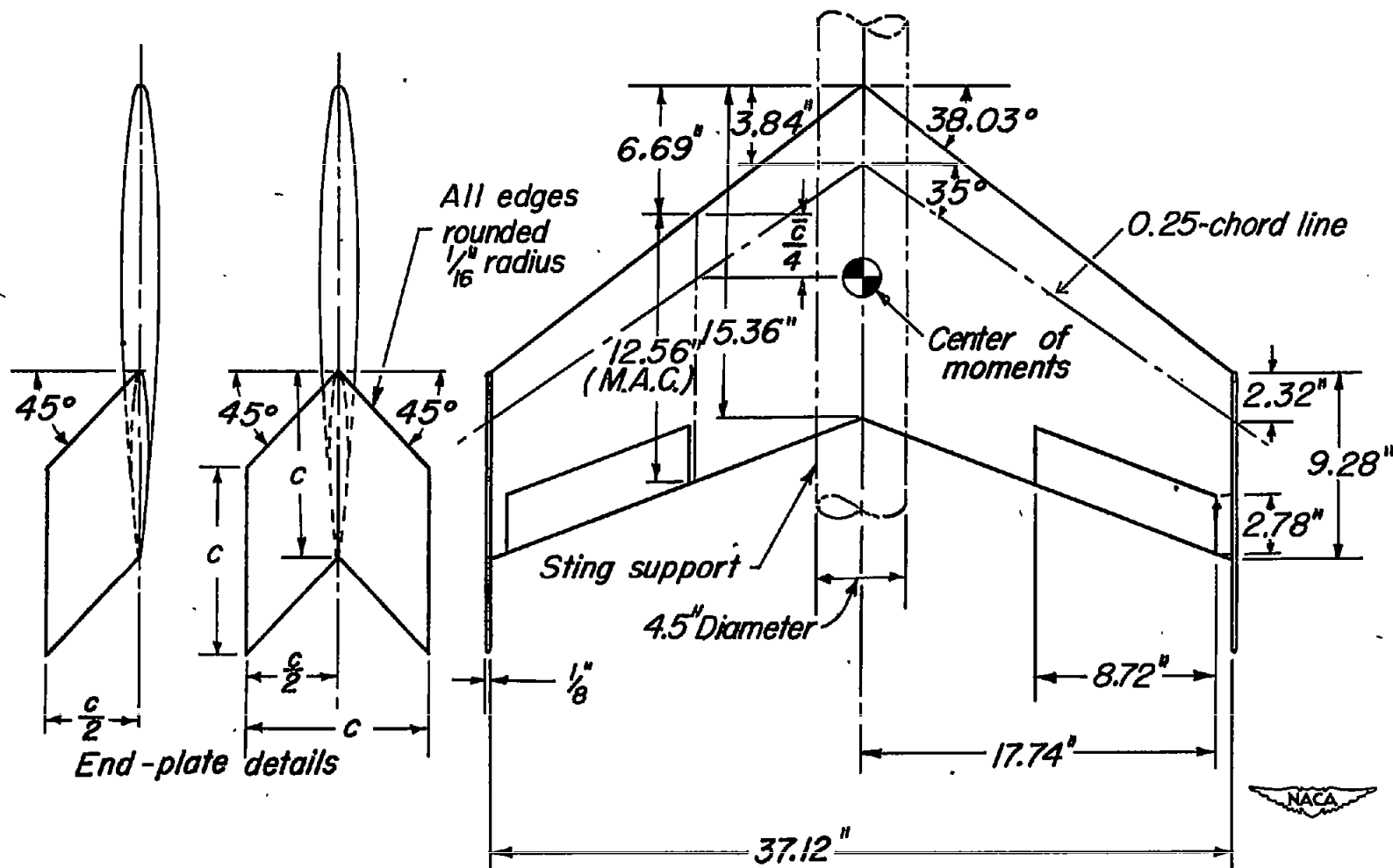
Figure 6.- Geometric characteristics of the 35° sweptback wing of aspect
ratio 3 and taper ratio 0.60 with two end-plate configurations.
S = 3.17 square feet.
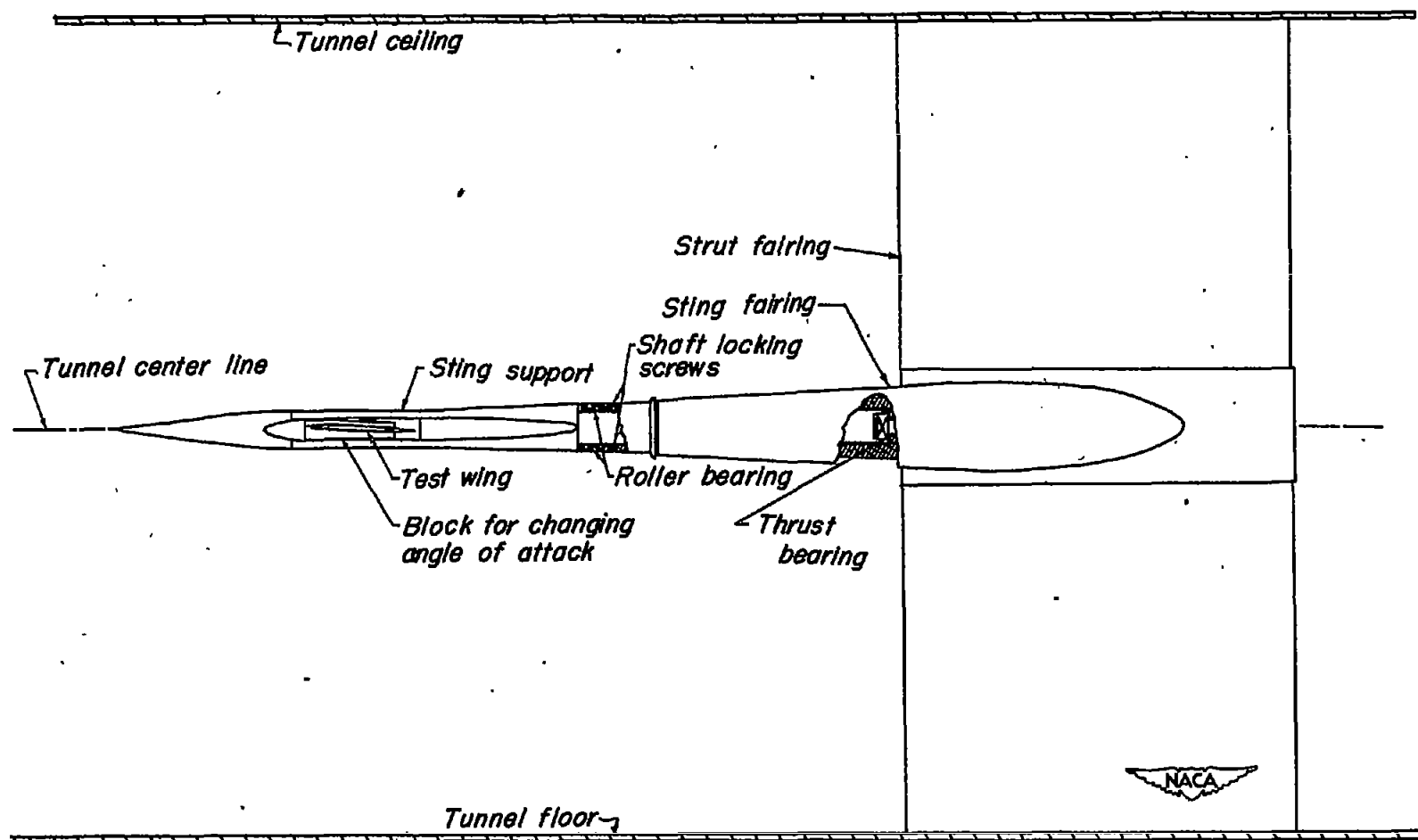
Figure 7.- Schematic drawing of the free-rolling sting mounted in the test
section of the Langley 300 MPH 7- by 10-foot tunnel.
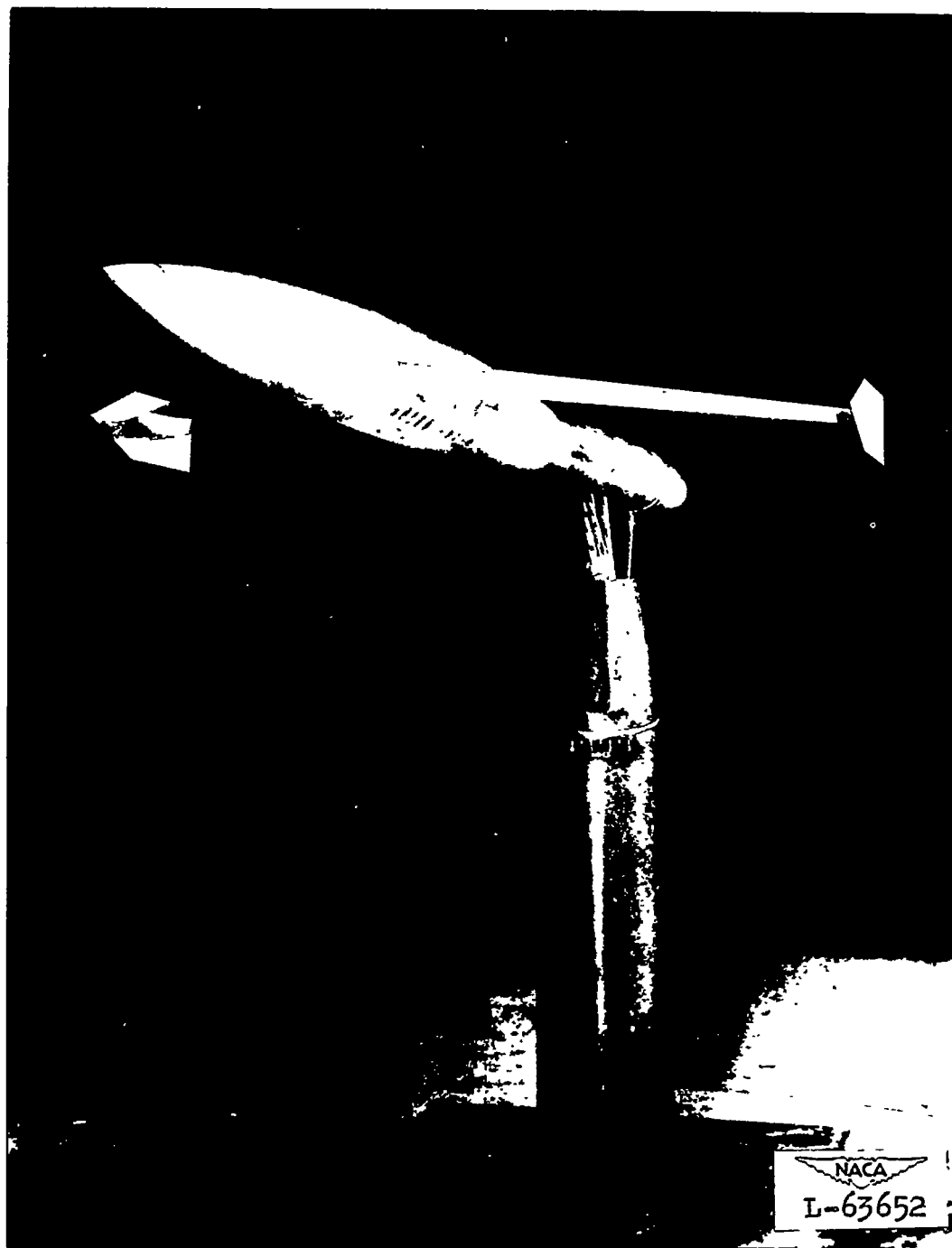
Figure 8.- The 46.7° sweptback wing of aspect ratio 4 with end plates mounted on sting-balance system in the Langley 300 MPH 7- by 10-foot tunnel.
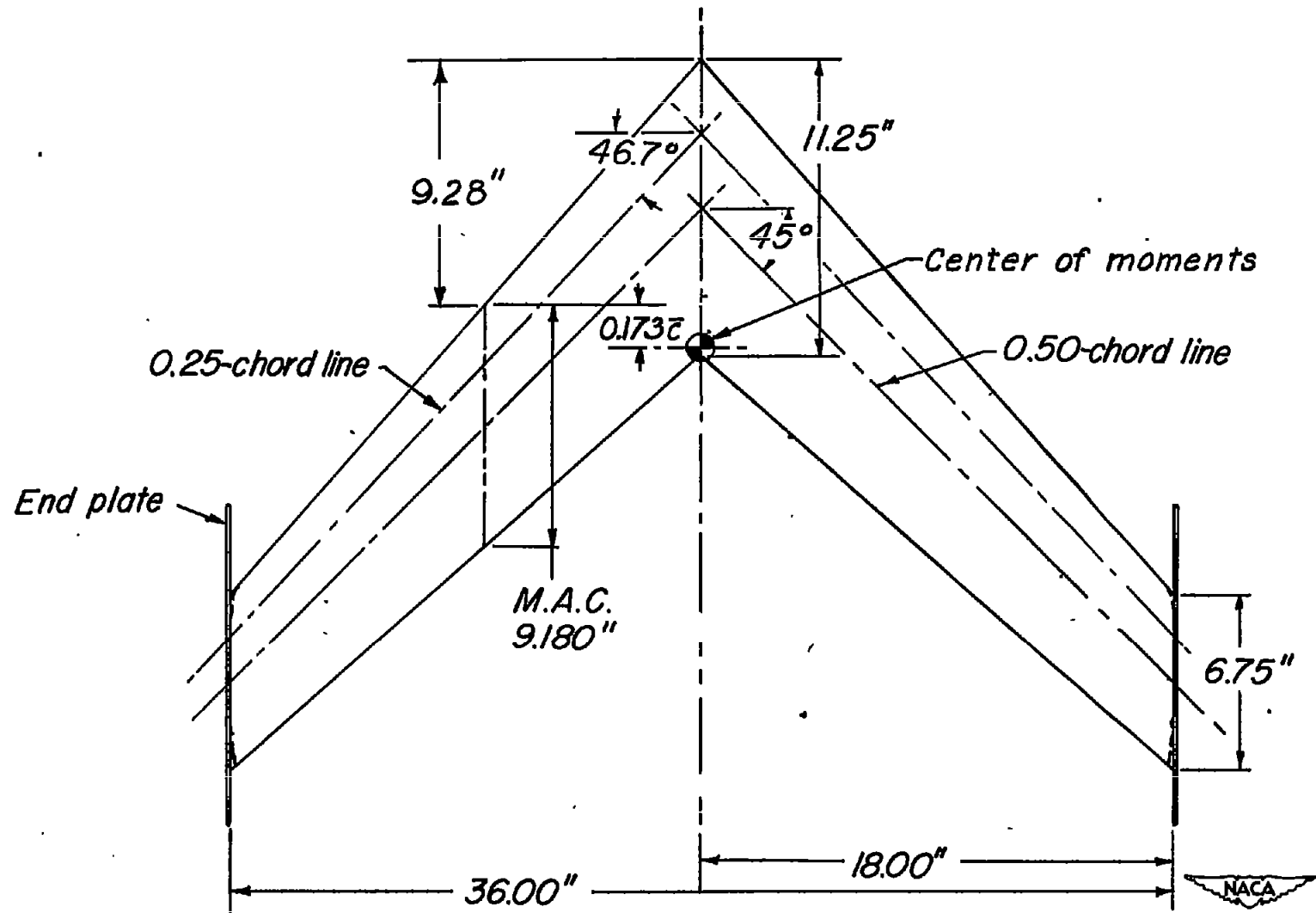
Figure 9.- Geometric characteristics of the 46.7° sweptback wing of aspect ratio 4 and taper ratio 0.60. S = 2.25 square feet.
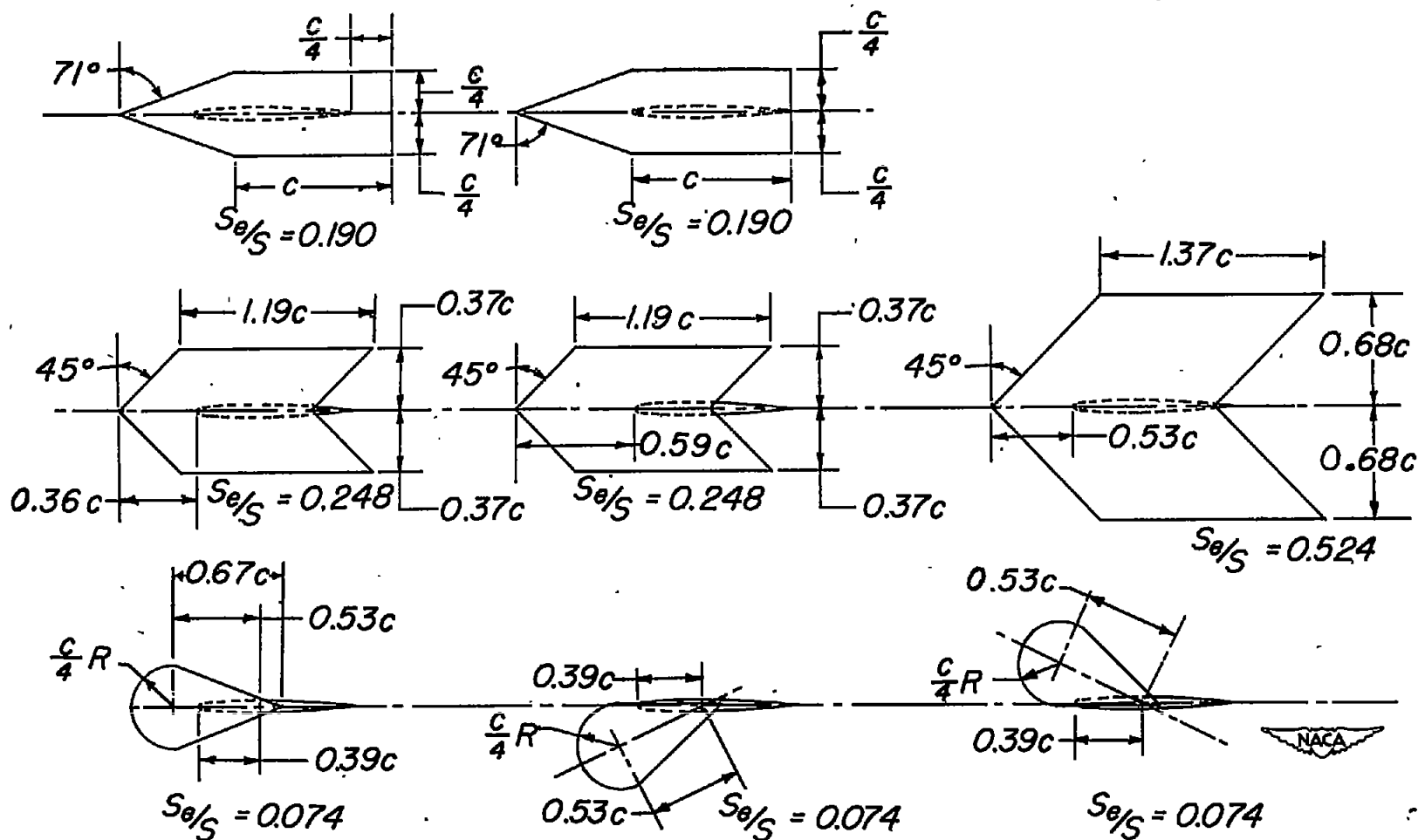
Figure 10.- Geometric characteristics of the various end plates investigated
on the 46.7° sweptback wing of aspect ratio 4.
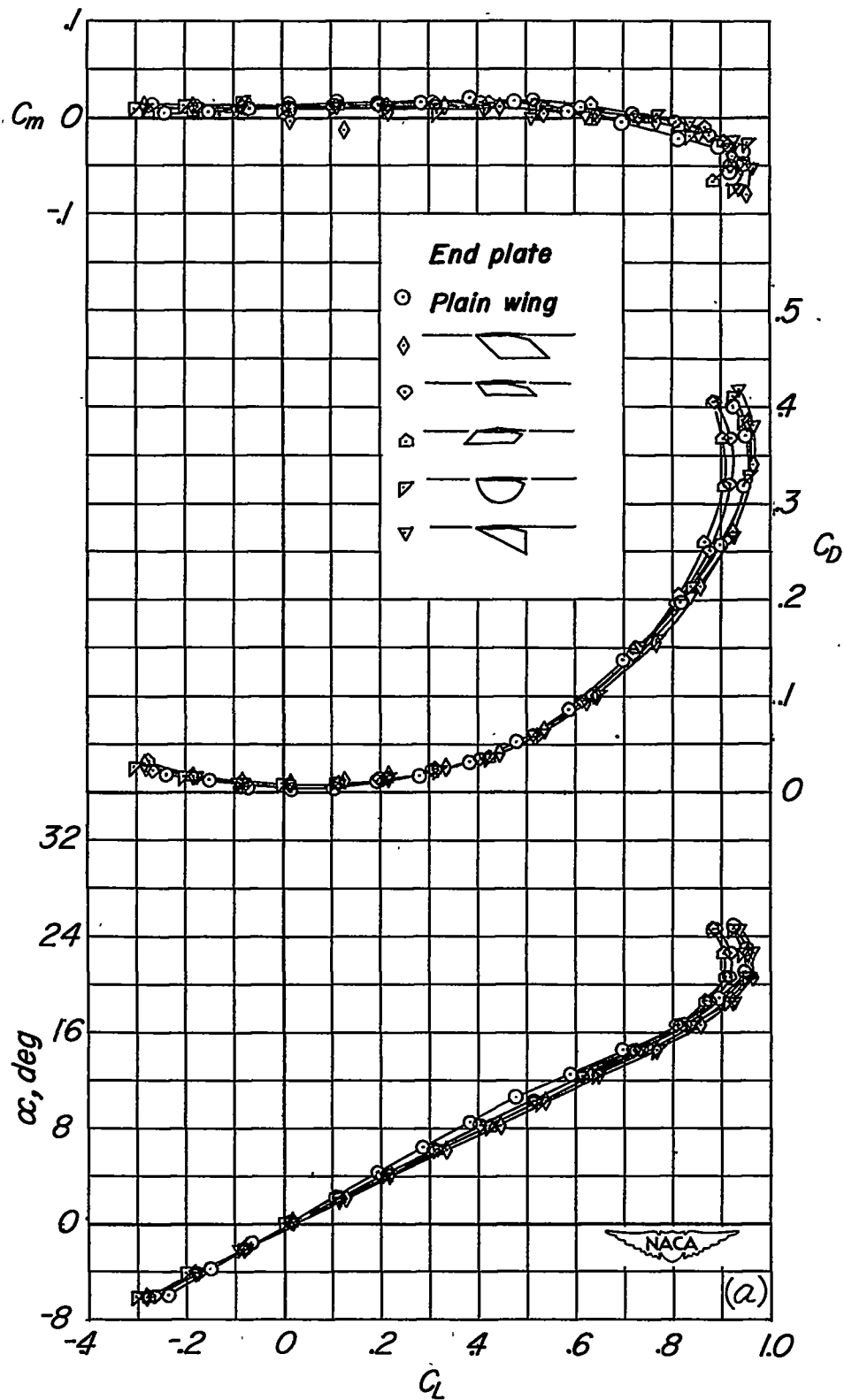
Figure 11.- Aerodynamic characteristics in pitch of the 45° sweptback wing
of aspect ratio 2 with and without various end plates.
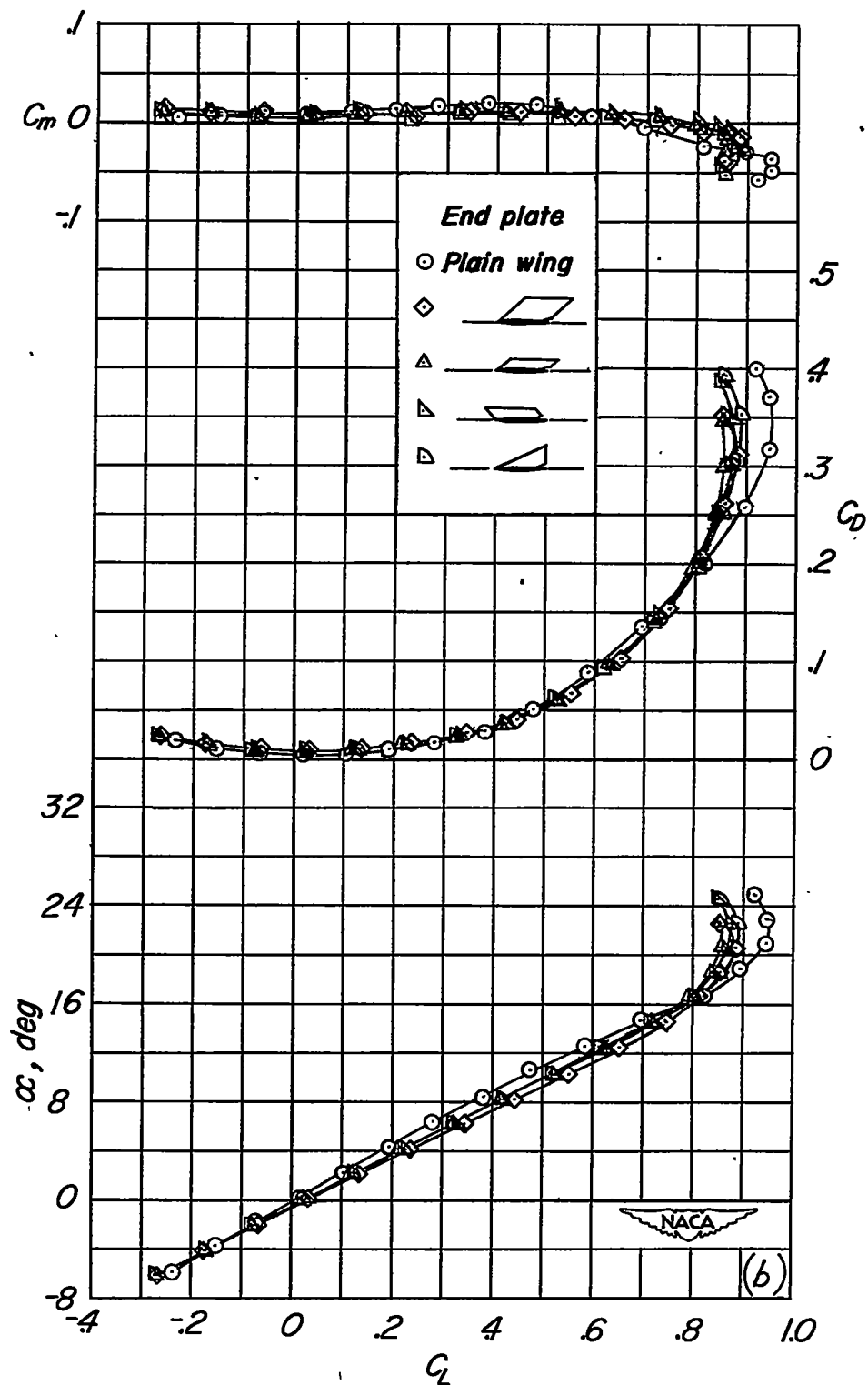
Figure 11.- Continued.
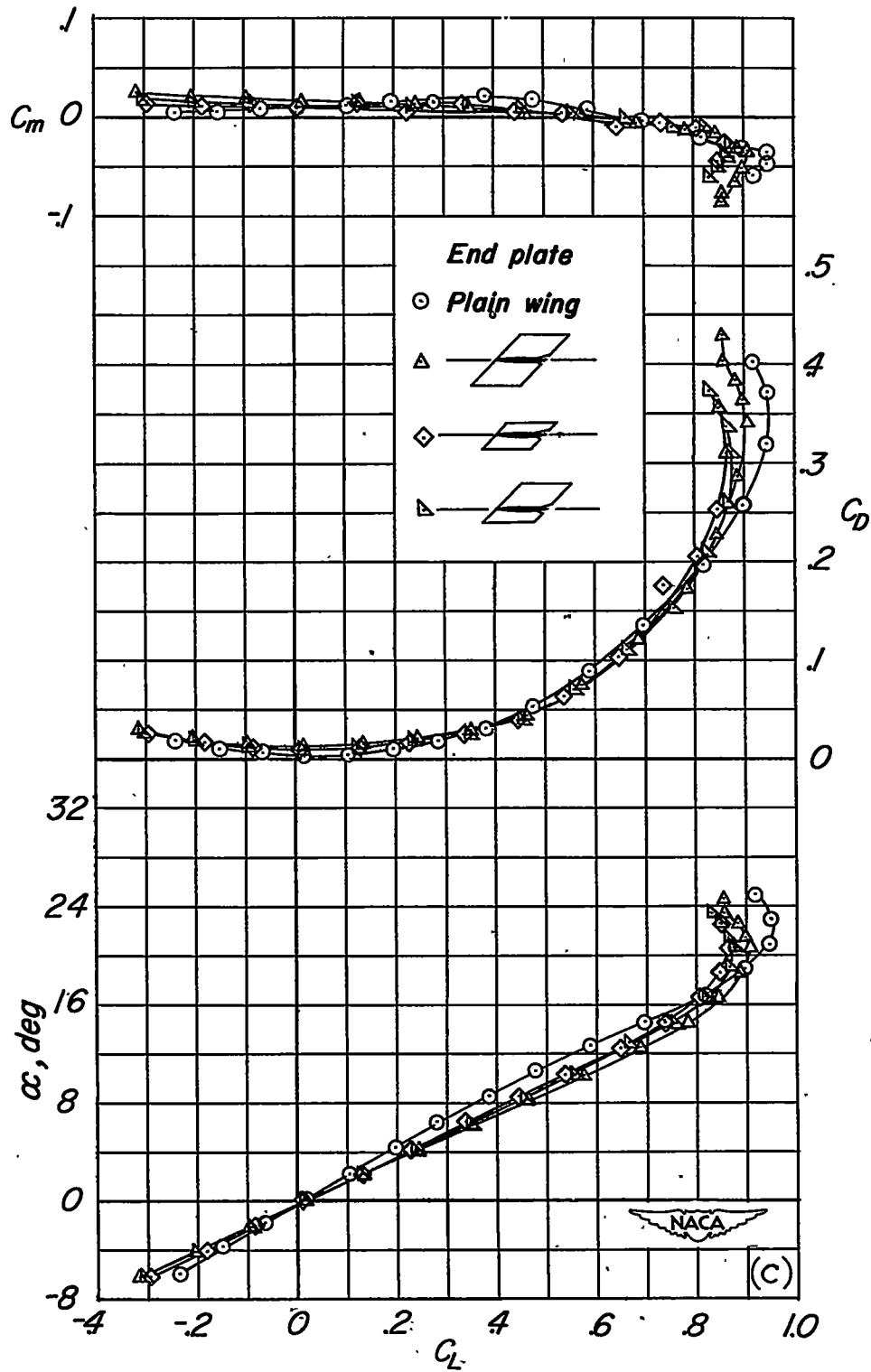
Figure 11.— Continued.
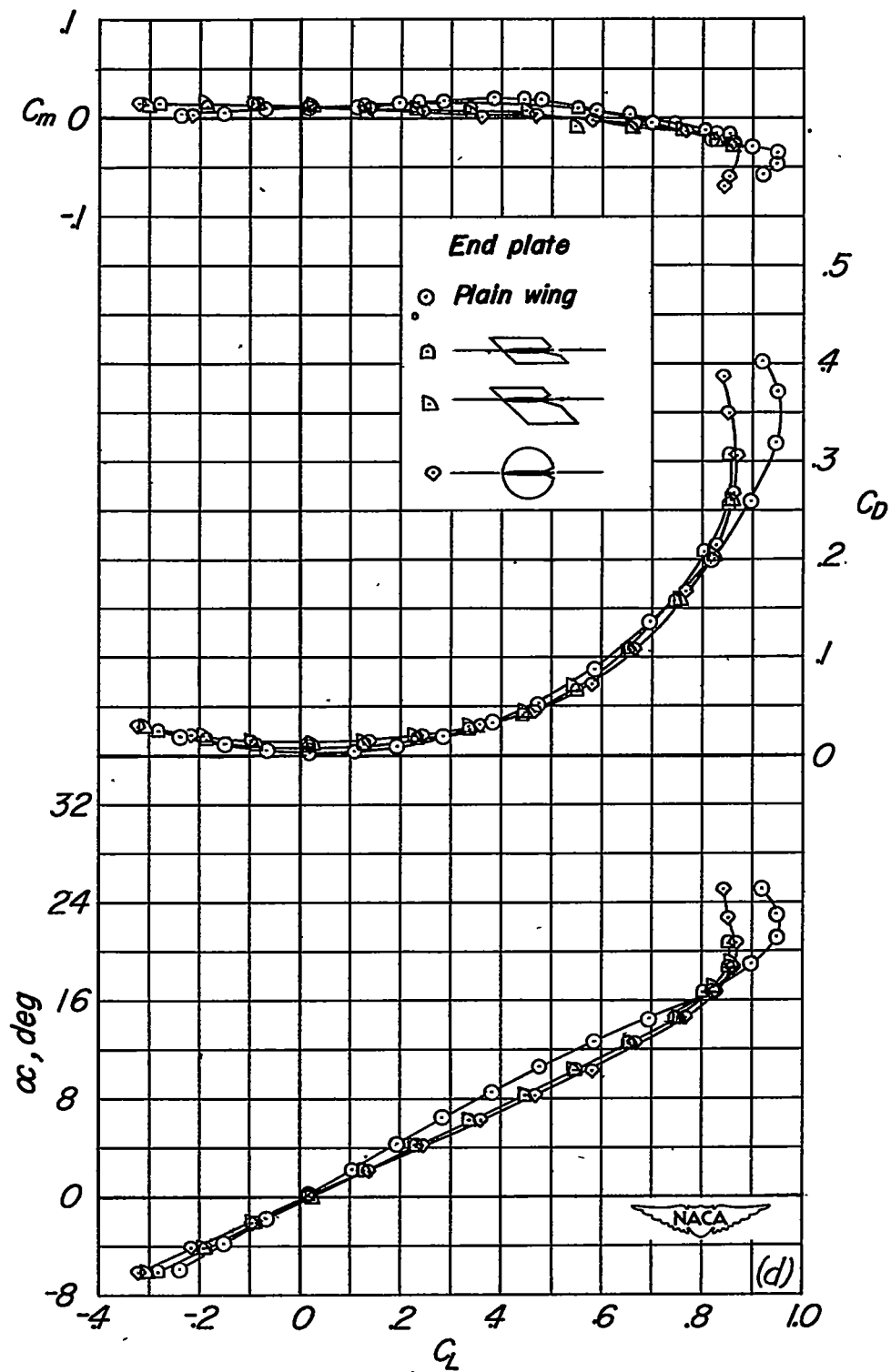
Figure 11.- Continued.
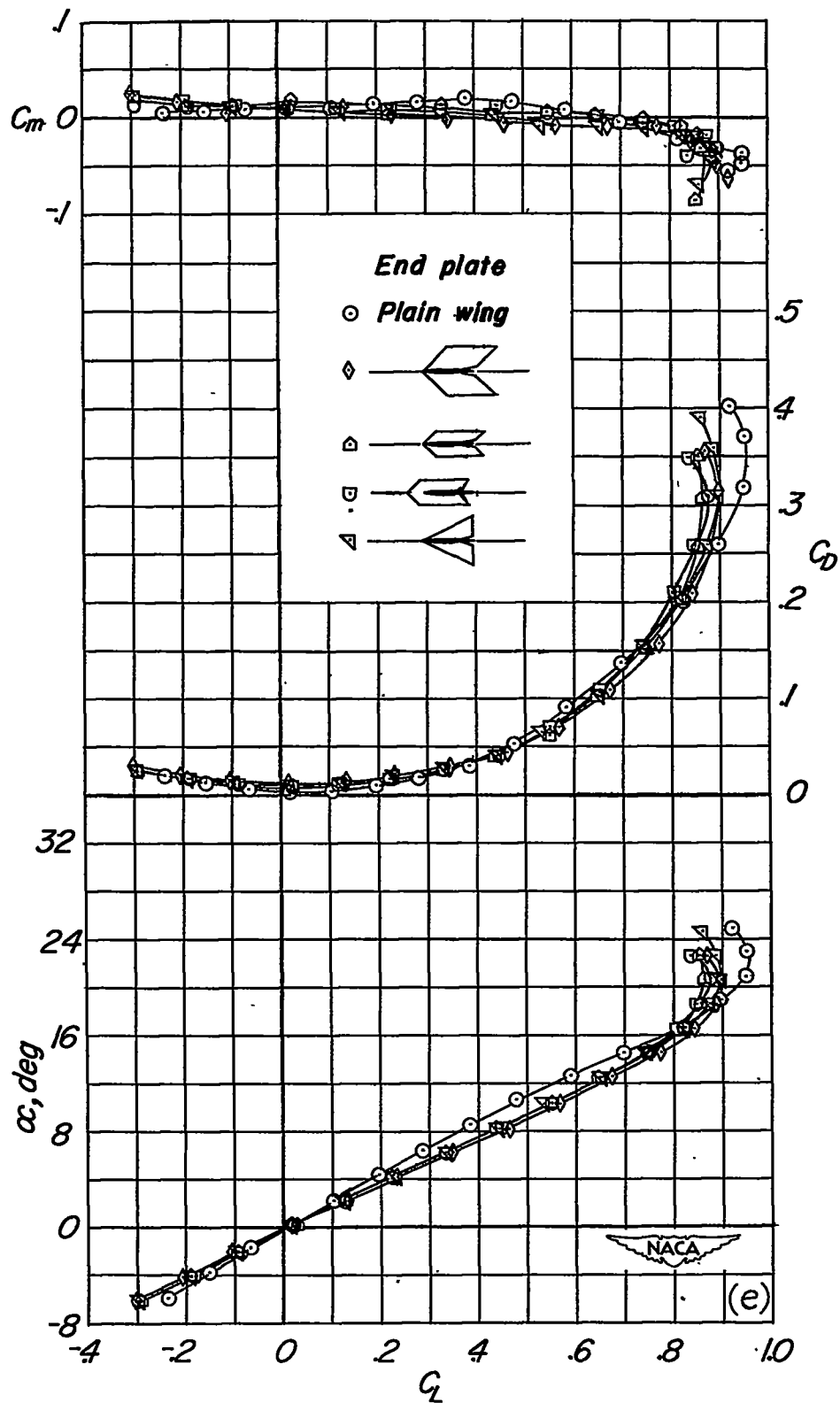
Figure 11.- Concluded.
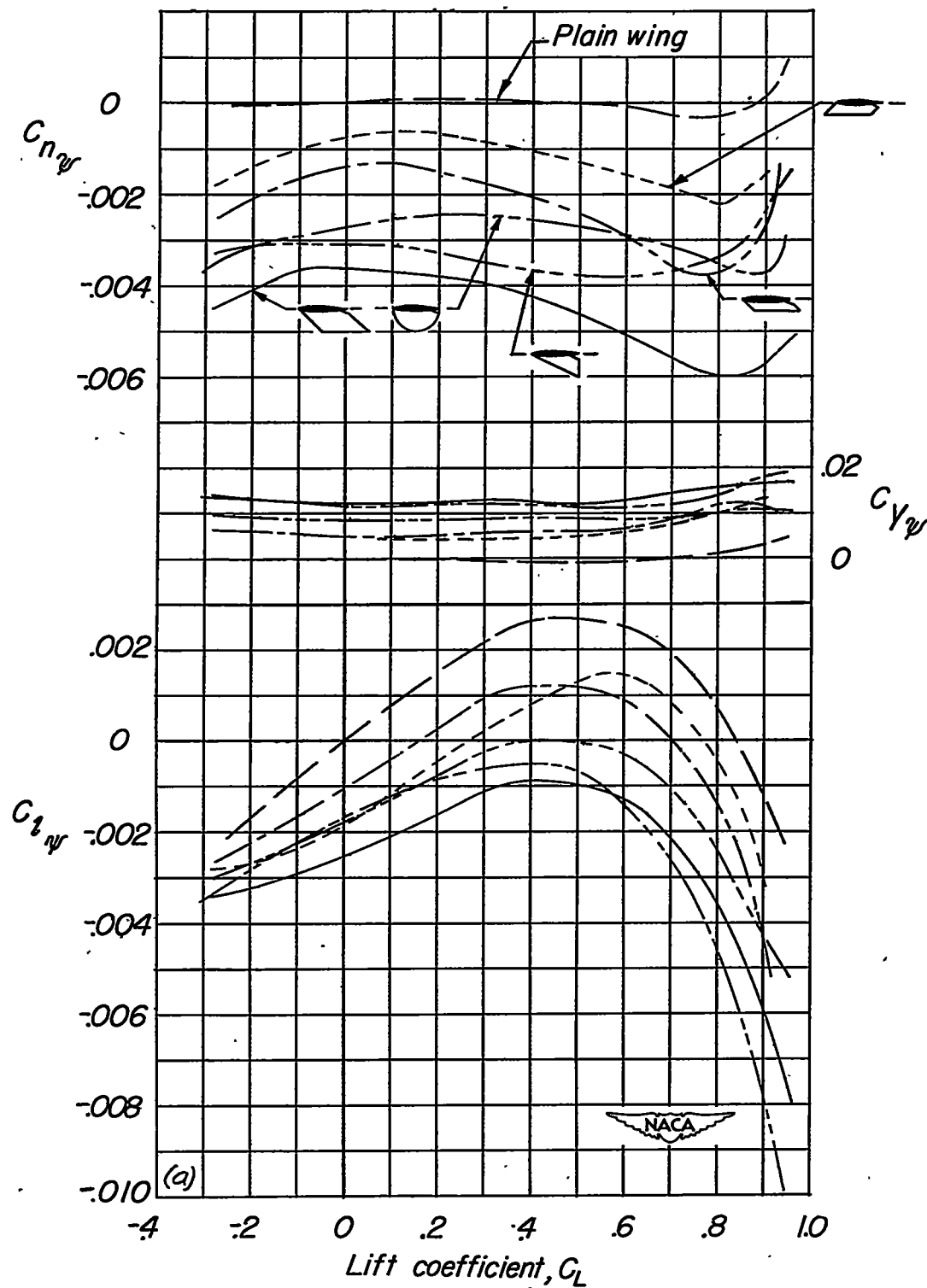
Figure 12.- Lateral-stability parameters in pitch of the 45° sweptback wing
of aspect ratio 2 with and without various end plates.
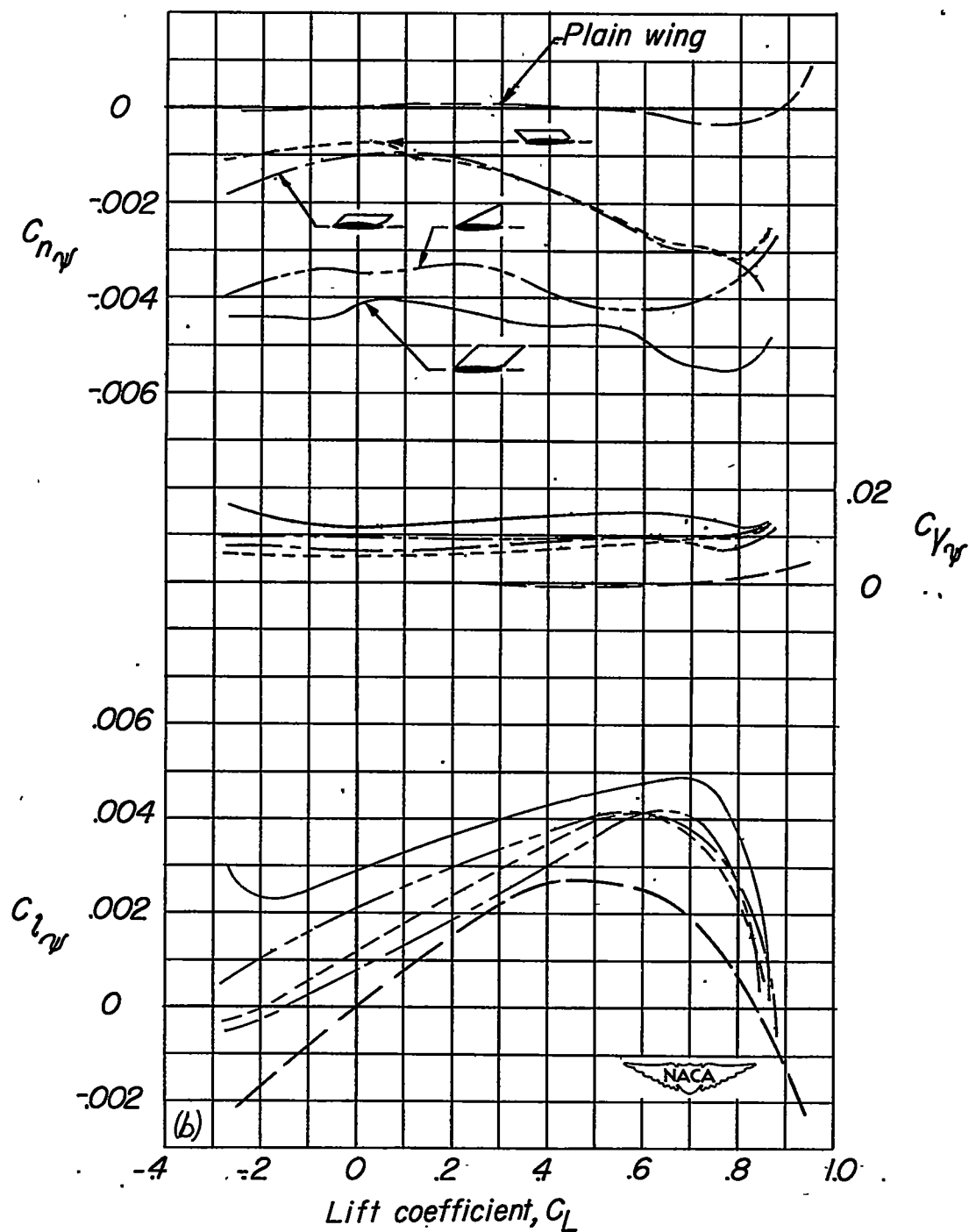
Figure 12.- Continued.
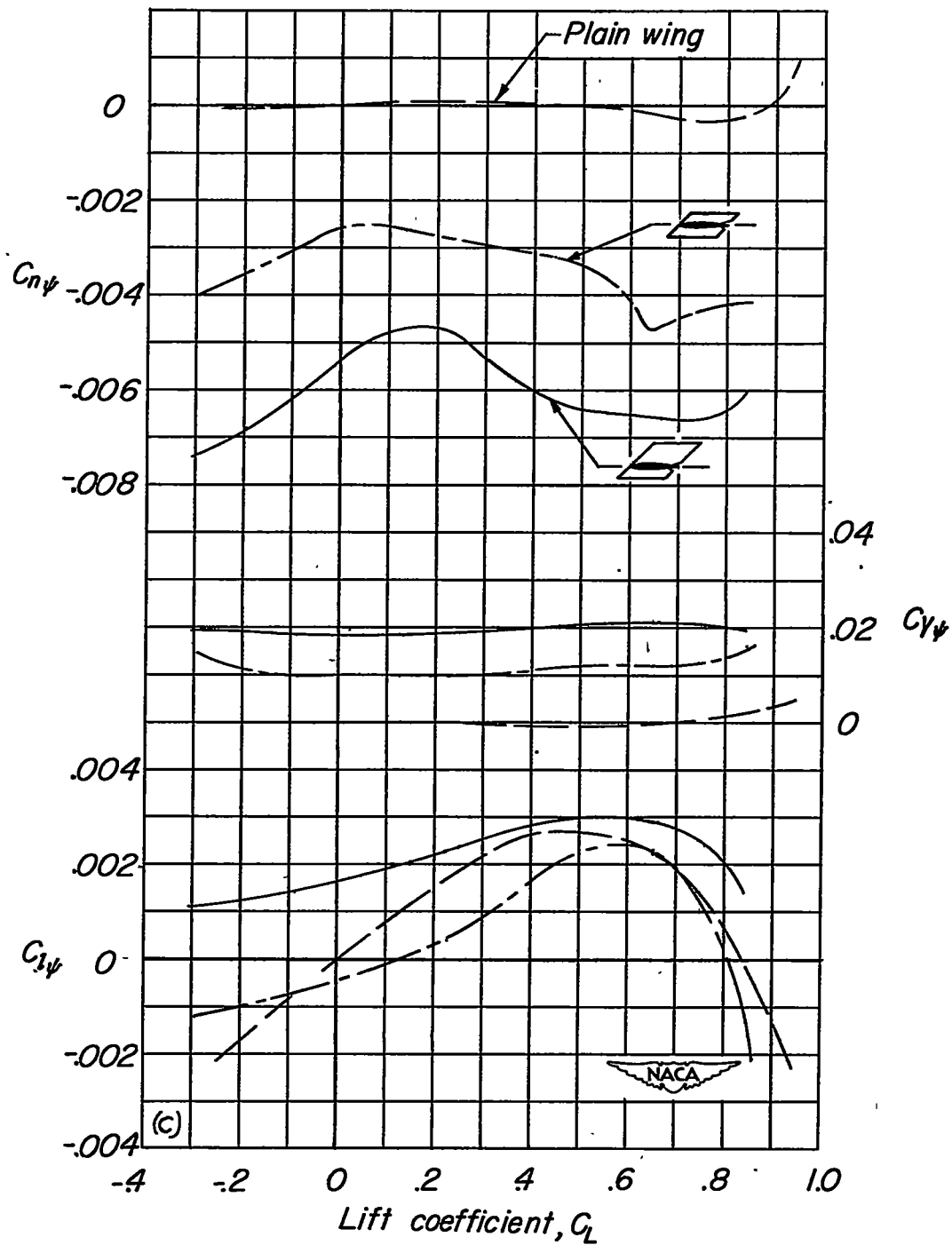
Figure 12.- Continued.
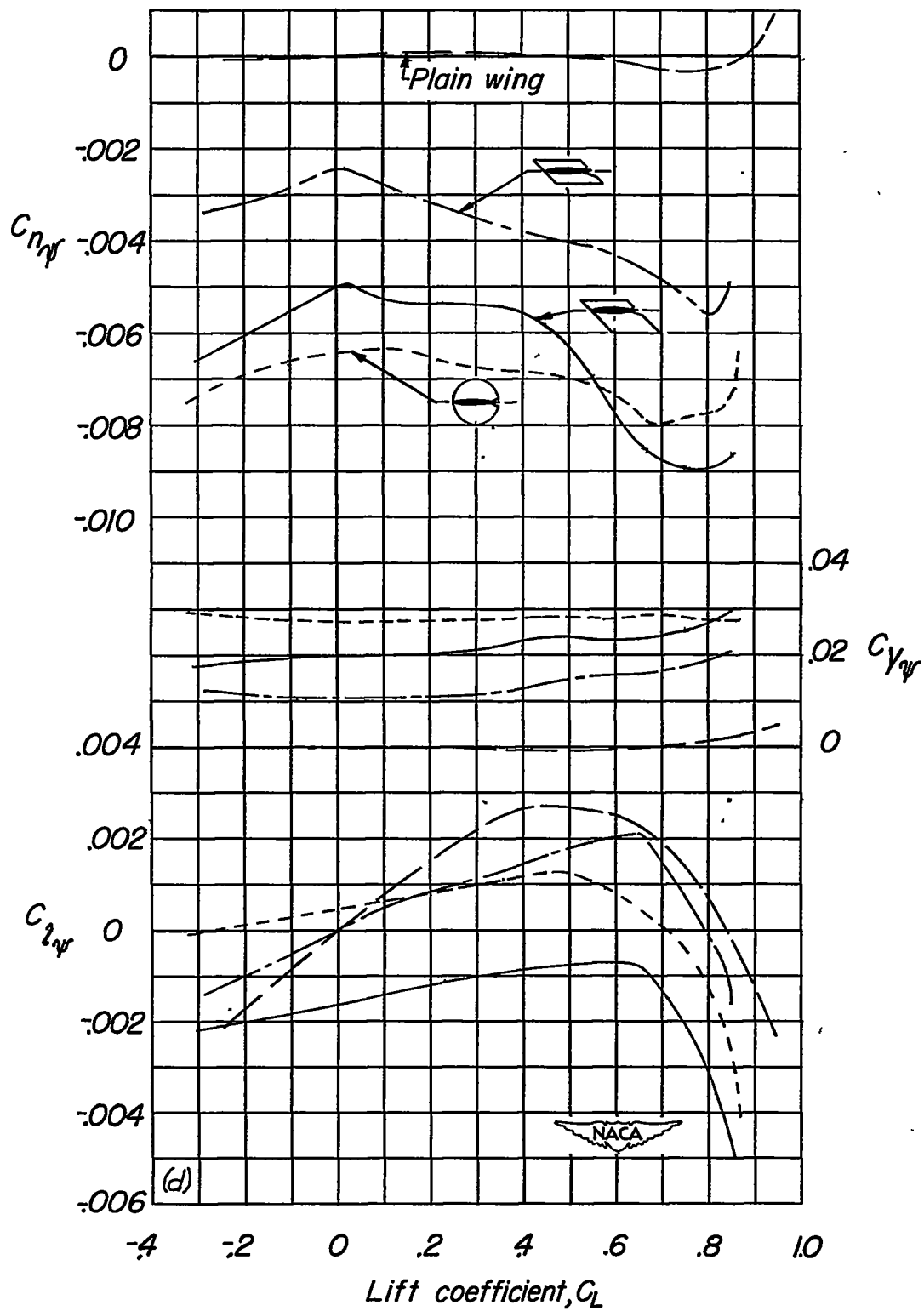
Figure 12.- Continued.
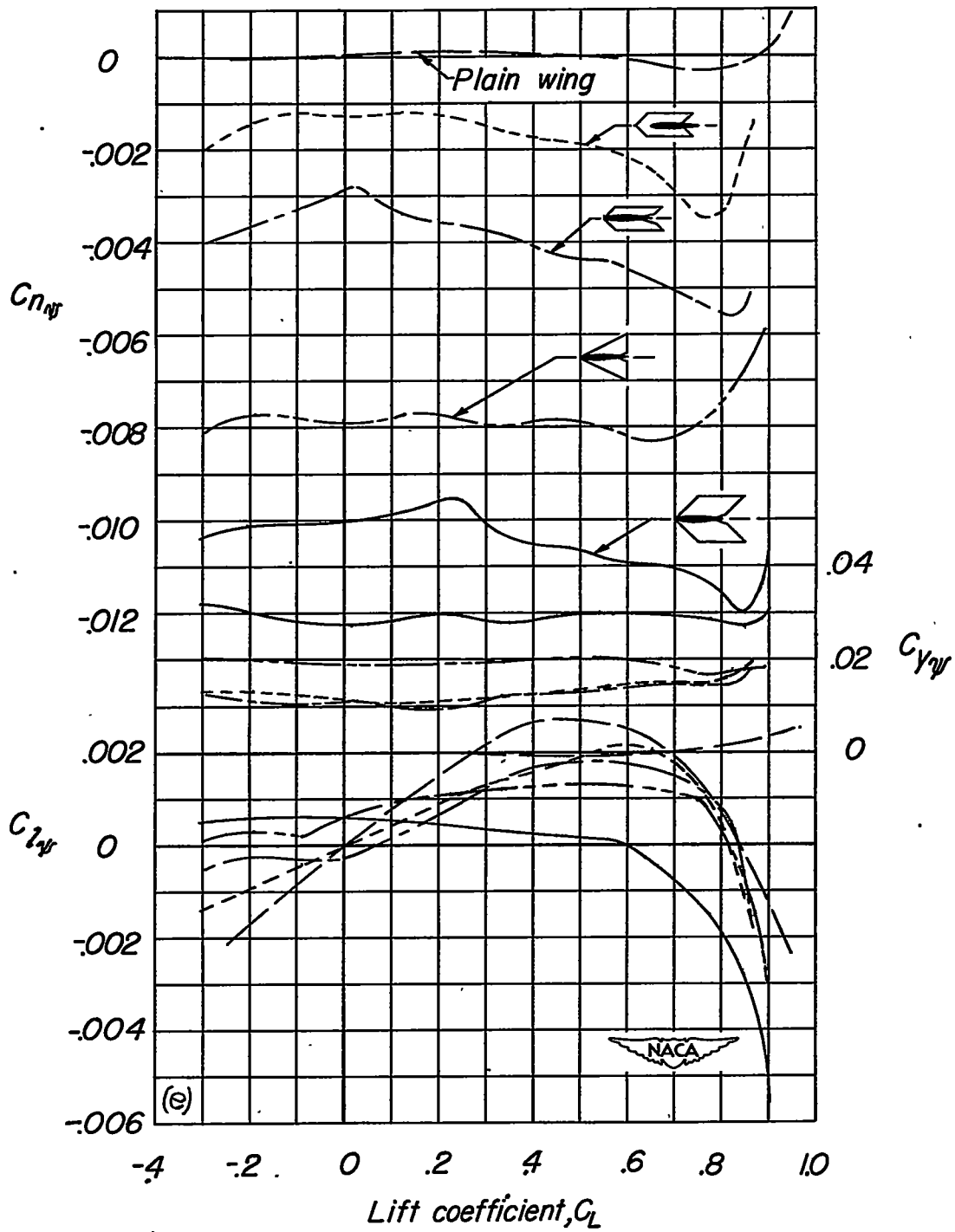
Figure 12.- Concluded.
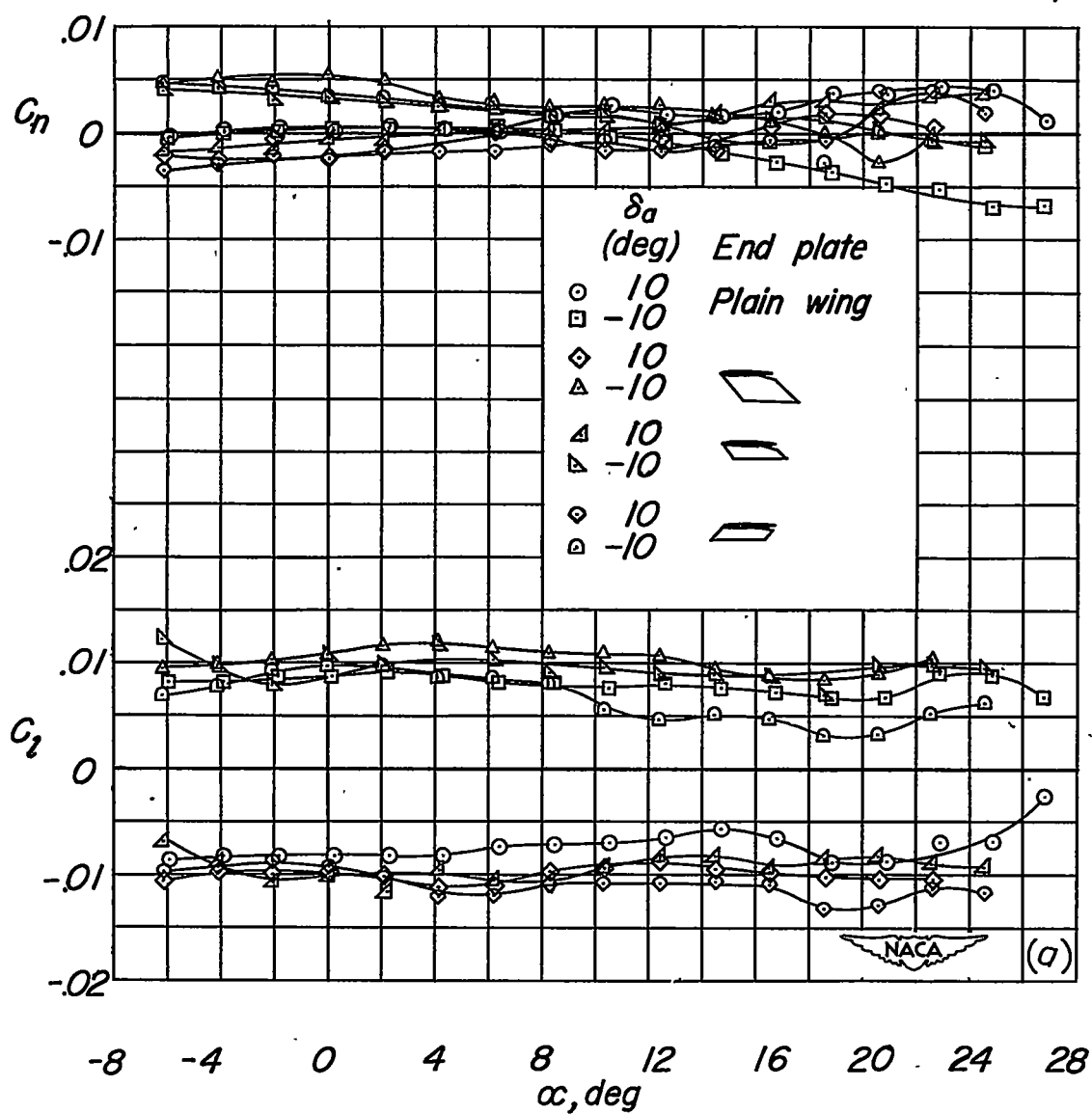
Figure 13.- Flap-type-aileron characteristics of the 45° sweptback wing of aspect ratio 2 with and without various end plates.

Figure 13.- Continued.
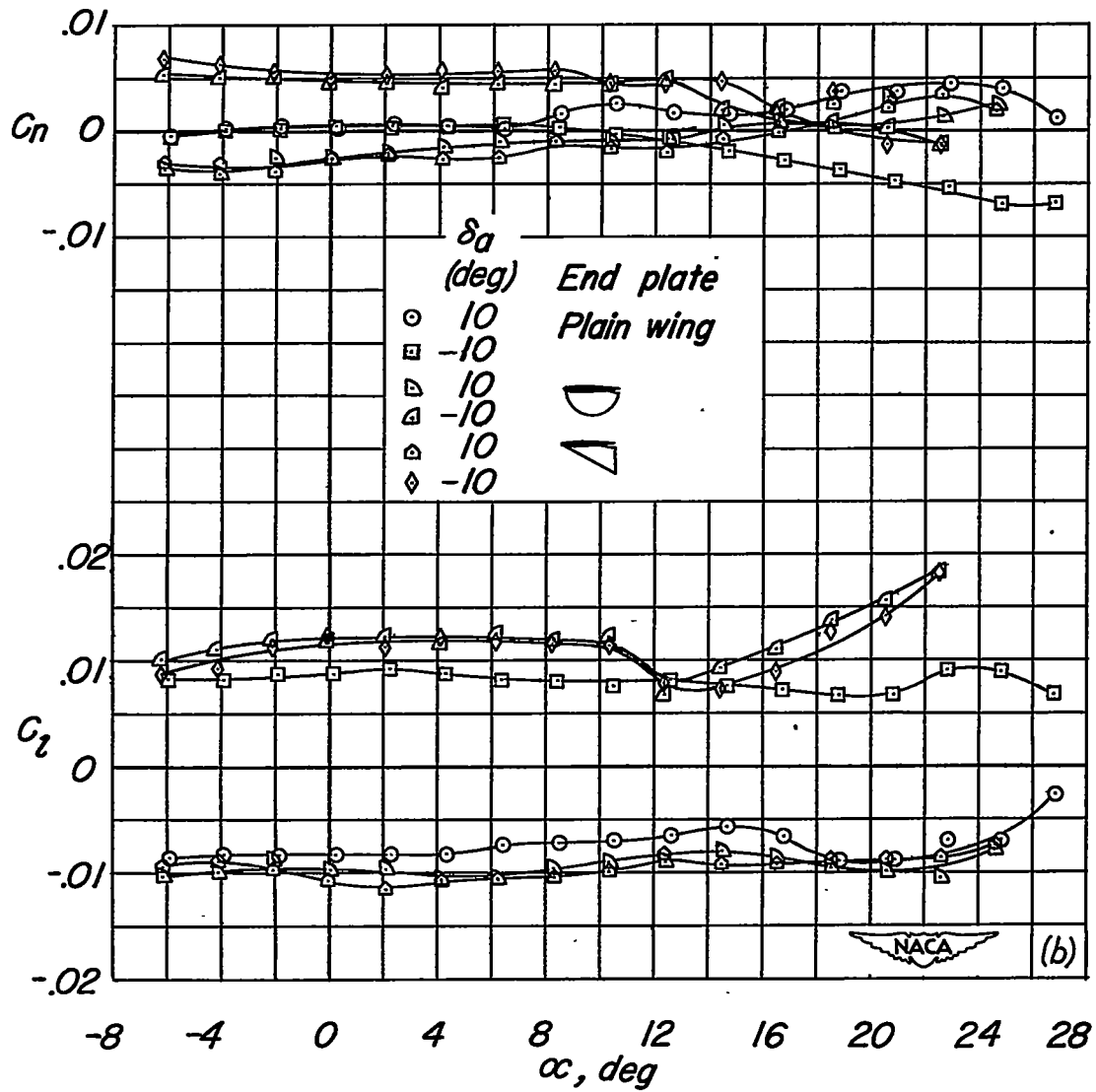
Figure 13.- Continued.
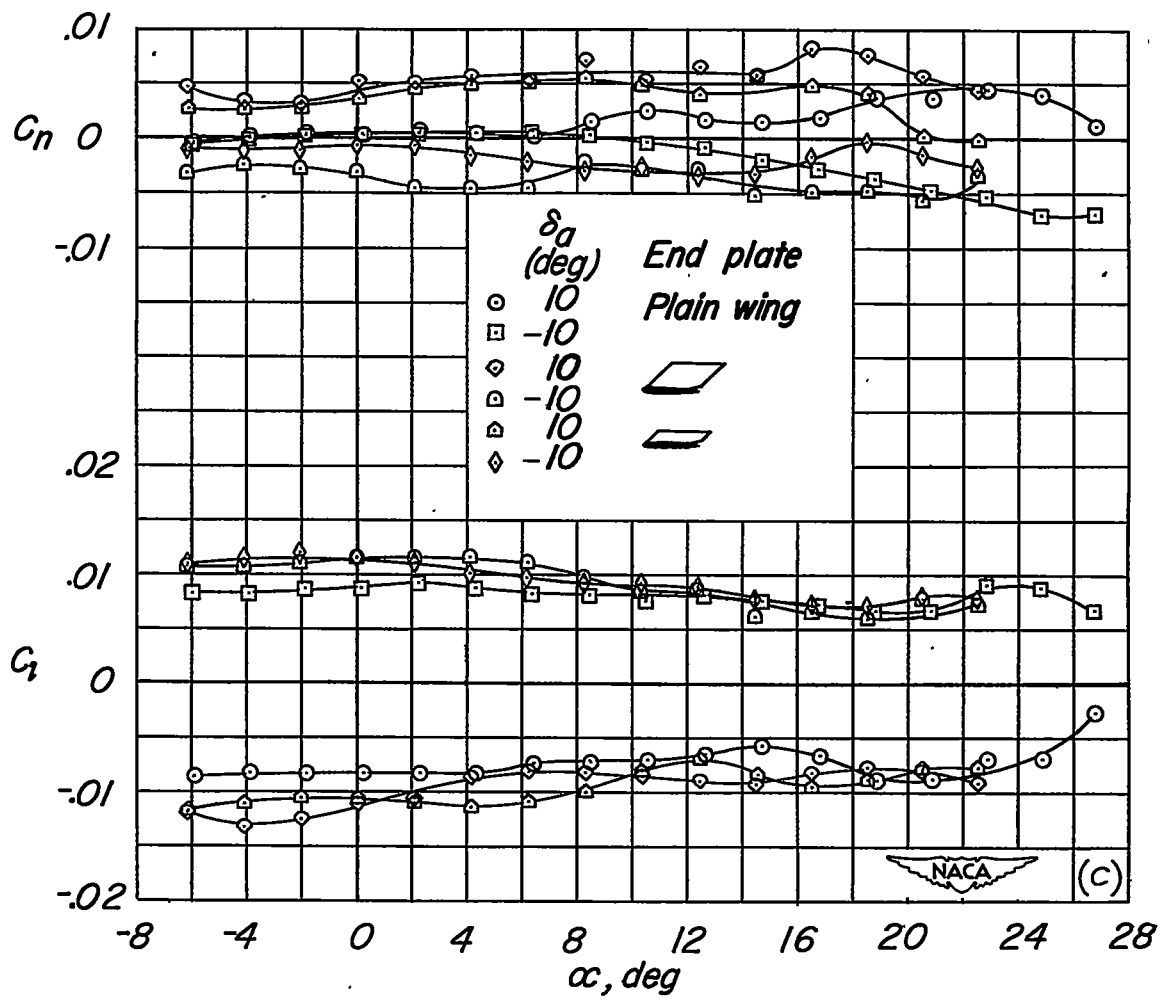
Figure 13.- Continued.
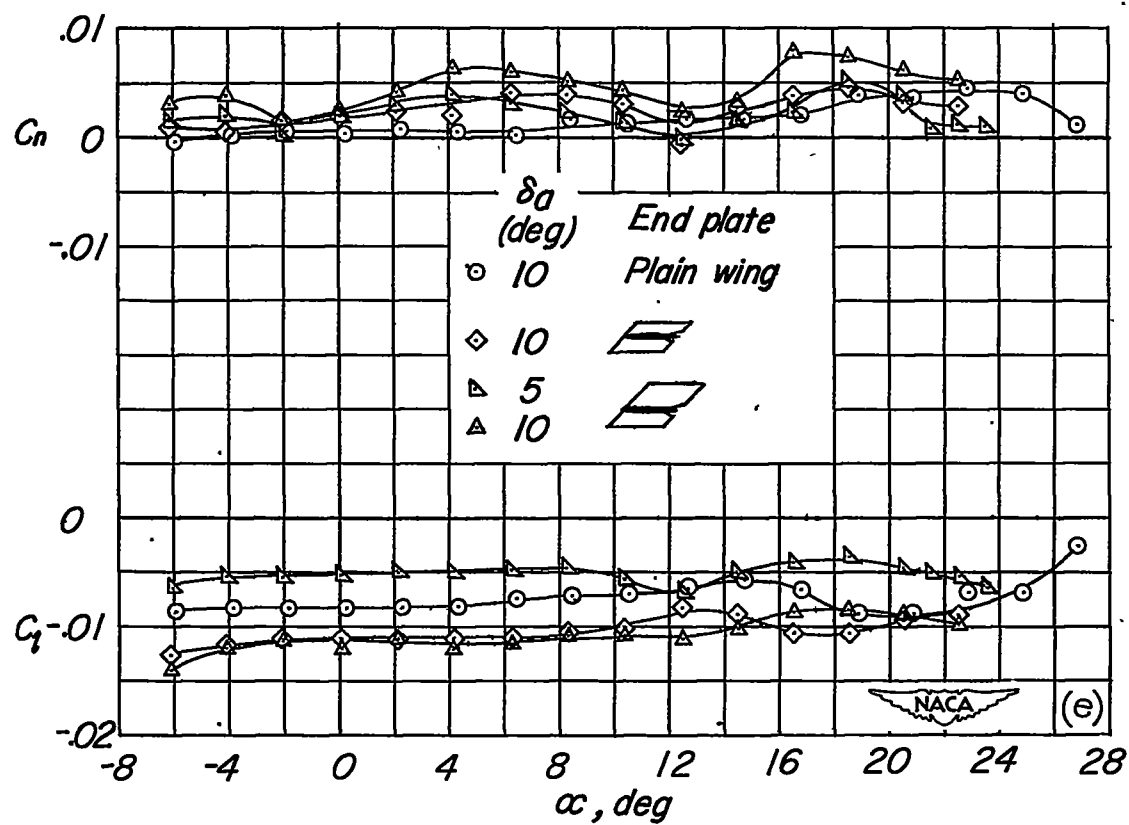
Figure 13.- Continued.
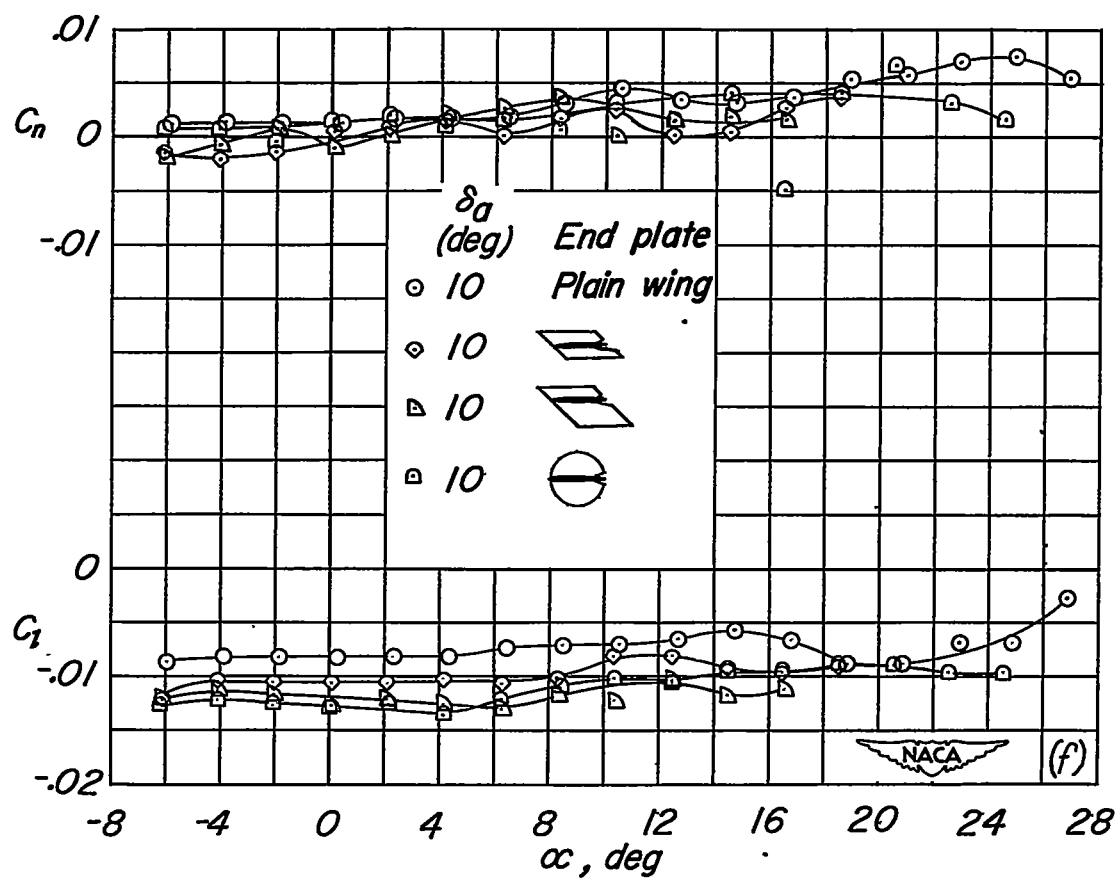
Figure 13.- Continued.
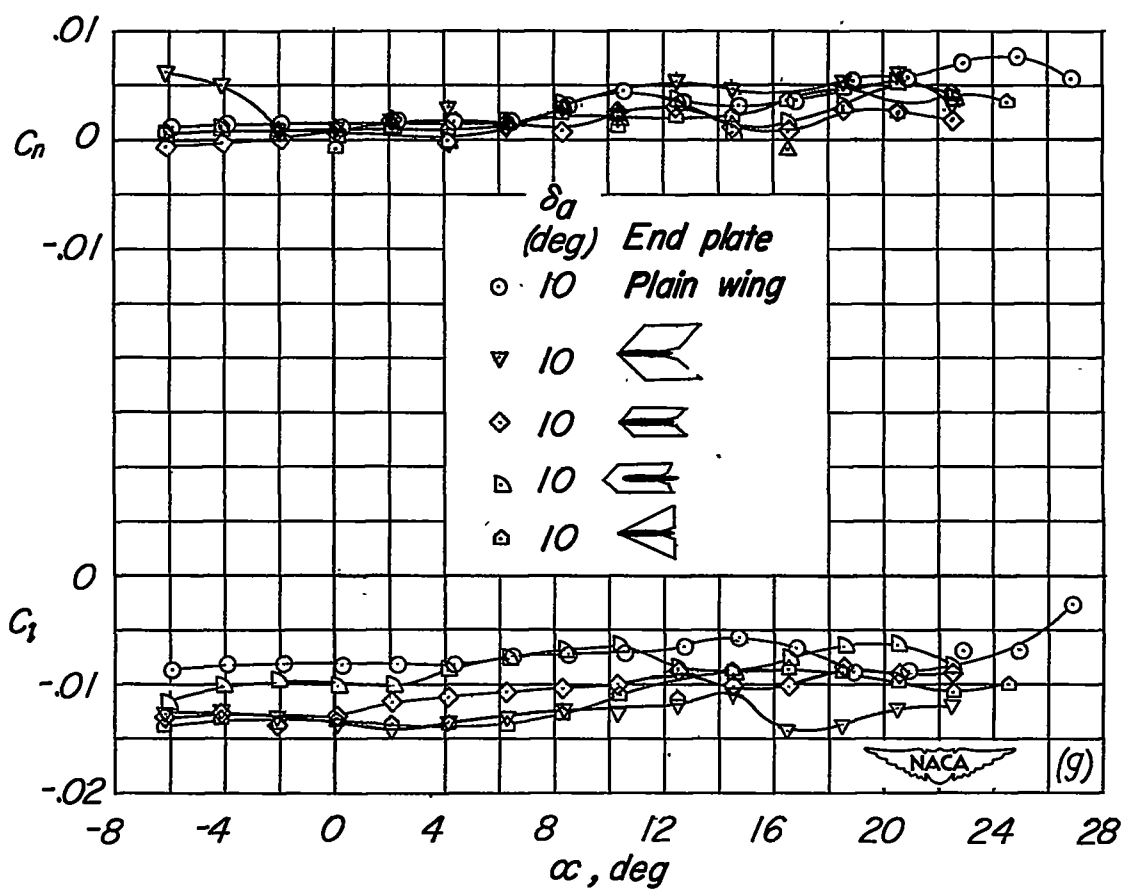
Figure 13.- Concluded.
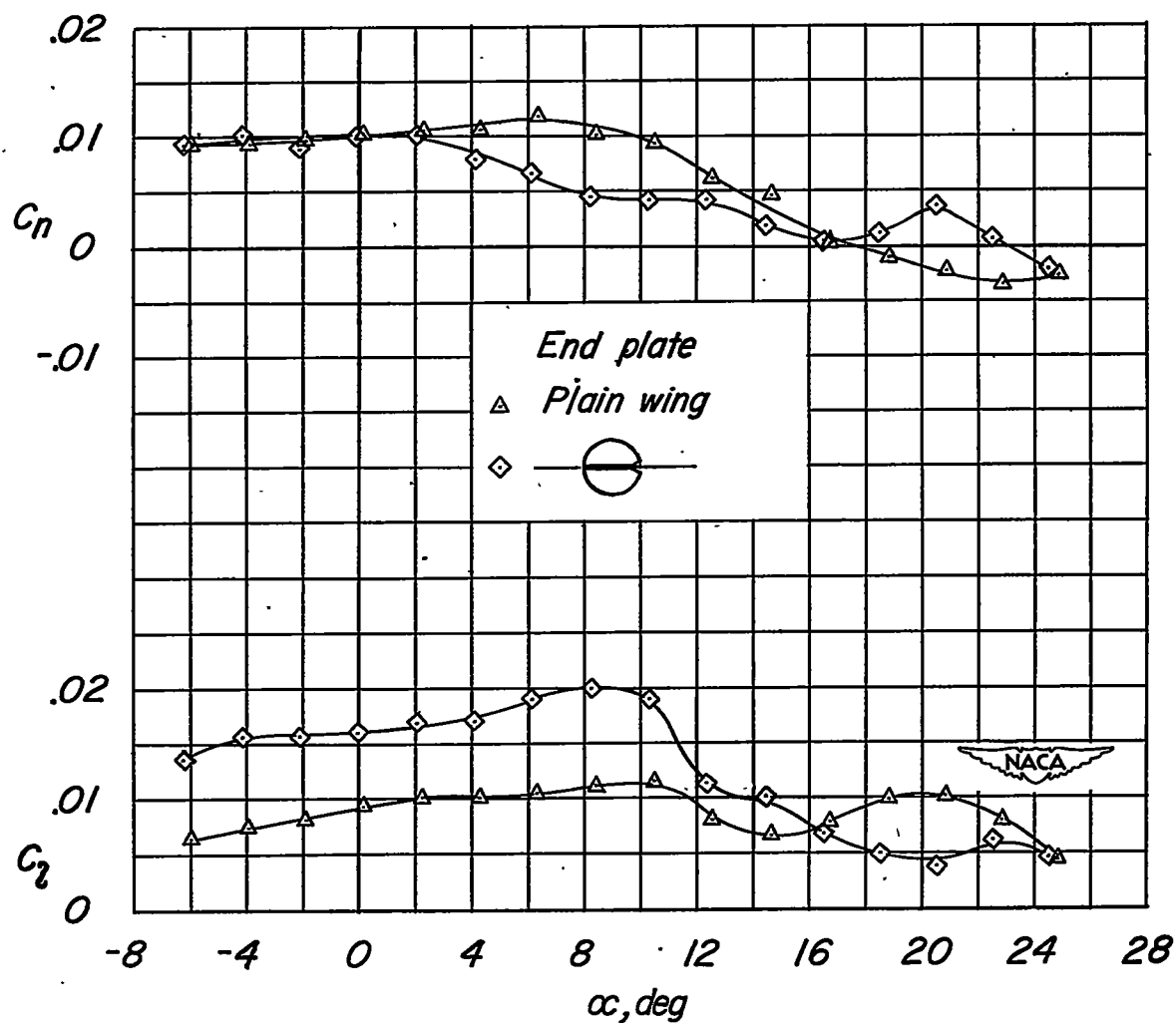
Figure 14.- Effect of an end plate on the rolling- and yawing-moment coefficients of the 45° sweptback wing of aspect ratio 2 with stepped spoiler ailerons.
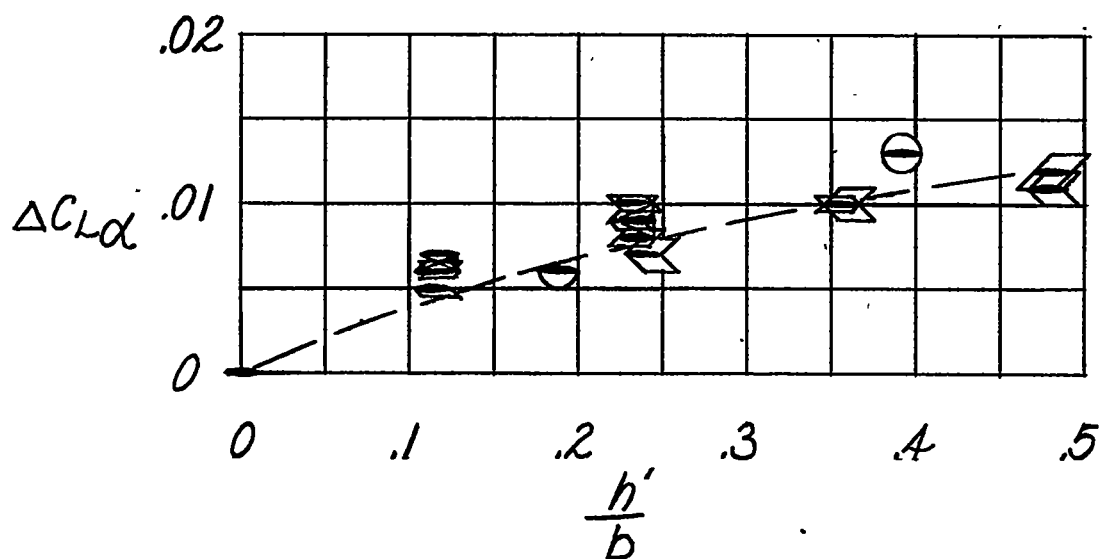
(a) $A = 2$; $\Lambda = 45^\circ$; $\lambda = 1.0$.

— — — *Theoretical (reference 7)*
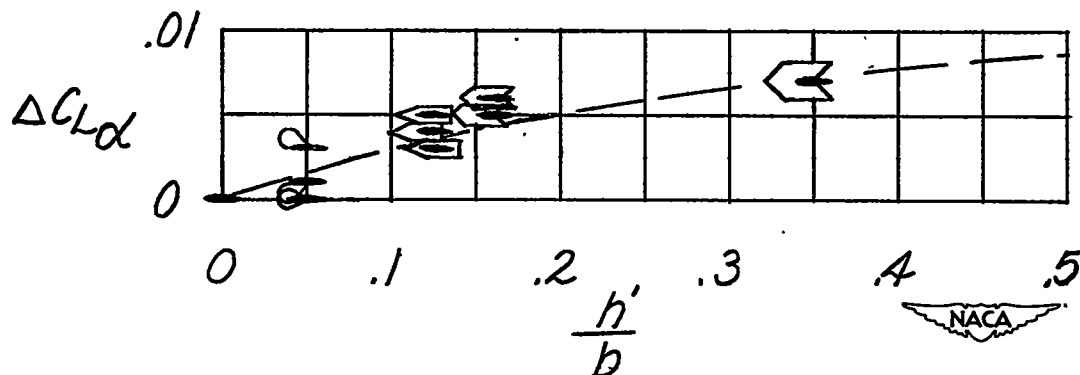
(b) $A = 4$; $\Lambda = 46.7^\circ$; $\lambda = 0.6$.

Figure 15.- The incremental lift-curve slopes of the wings of aspect ratios 2 and 4 with various end plates. $C_L = 0$.
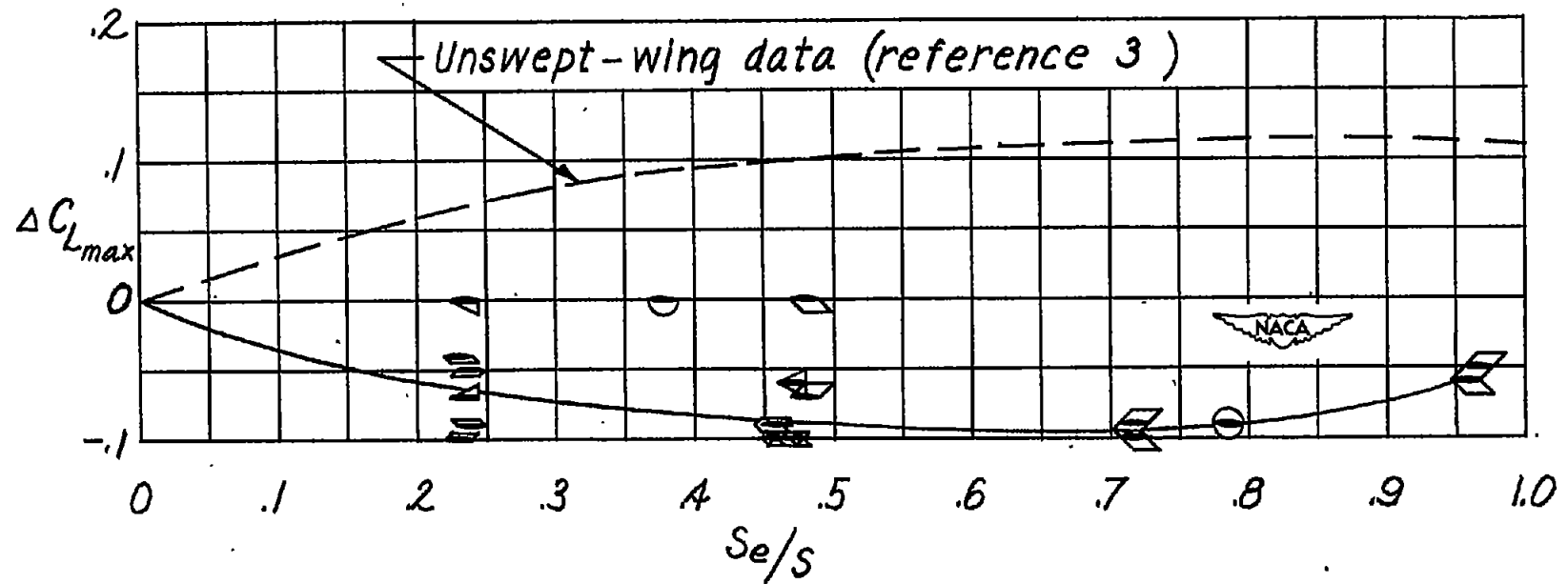
Figure 16.- The incremental values of maximum lift coefficient of the 45° sweptback wing of aspect ratio 2.

(a) A = 2; Λ = 45°; λ = 1.0.
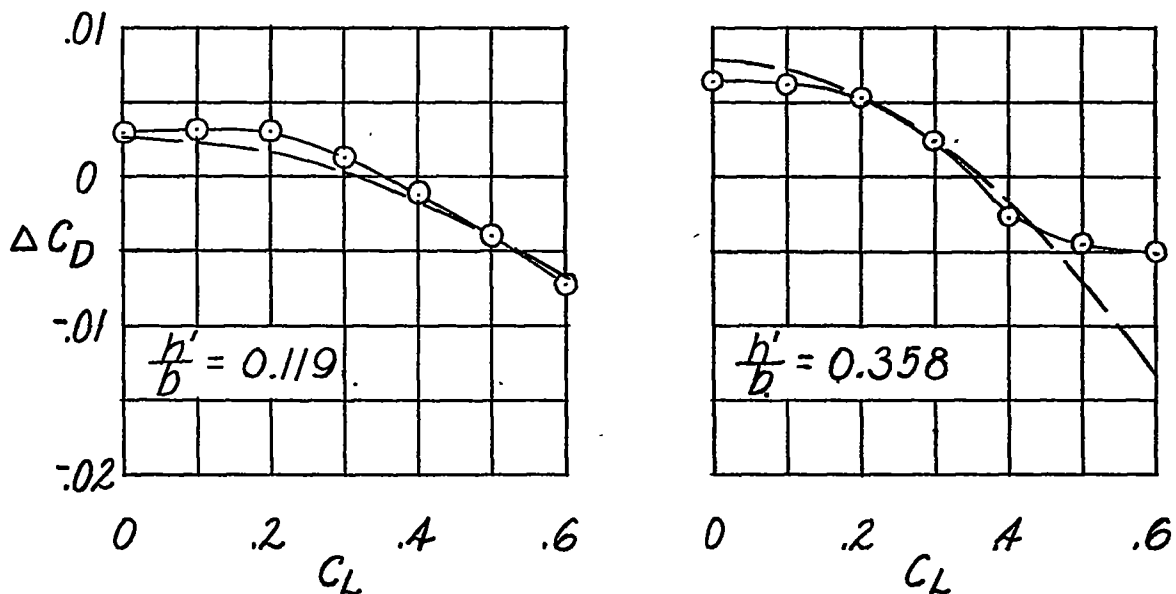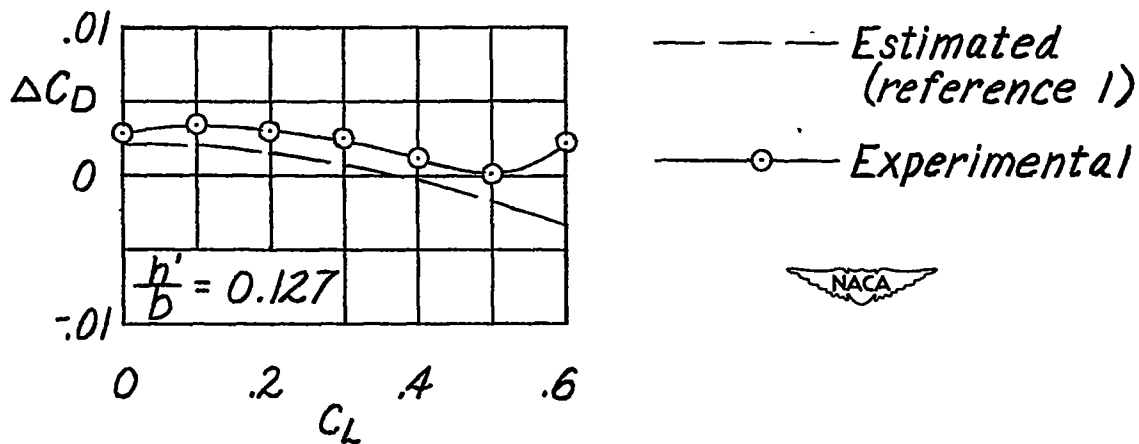
(b) A = 4; Λ = 46.7°; λ = 0.6.

Figure 17.- The incremental drag coefficients of the wings with various end plates.
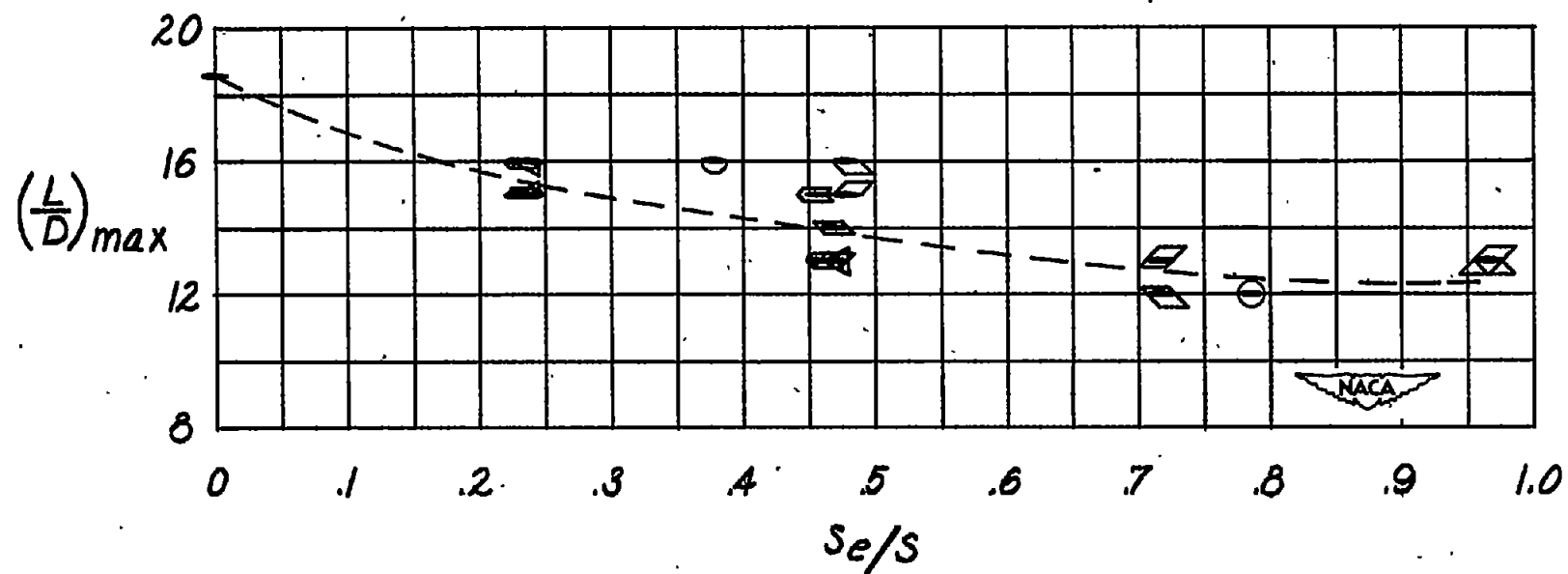
Figure 18.- The maximum lift-drag ratios of the 45° sweptback wing of aspect ratio 2.
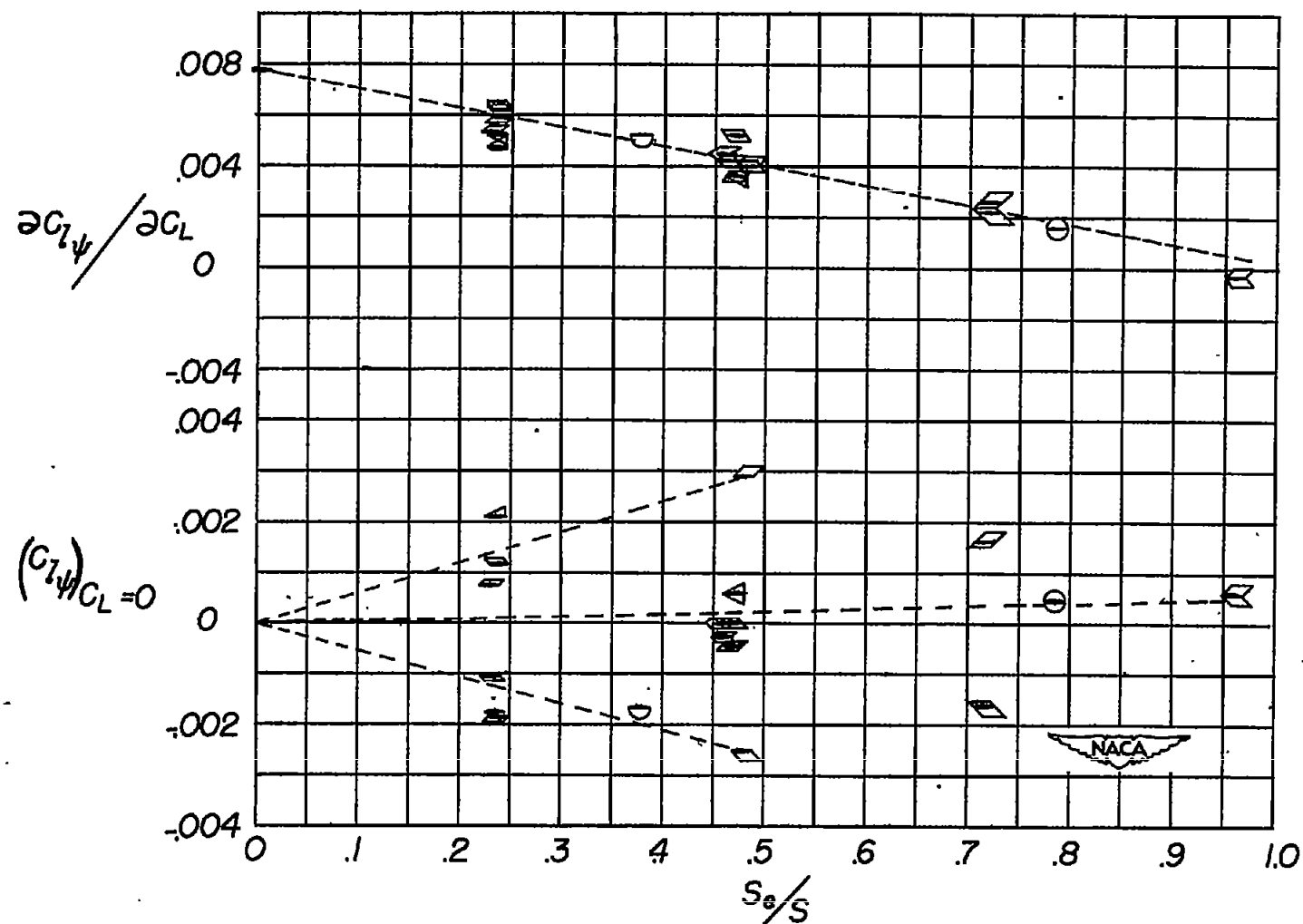
Figure 19.— Lateral-stability parameters $\left(C_{l_\psi}\right)_{C_L=0}$ and $\partial C_{l_\psi}/\partial C_L$ of the 45° sweptback wing of aspect ratio 2 with various end plates.
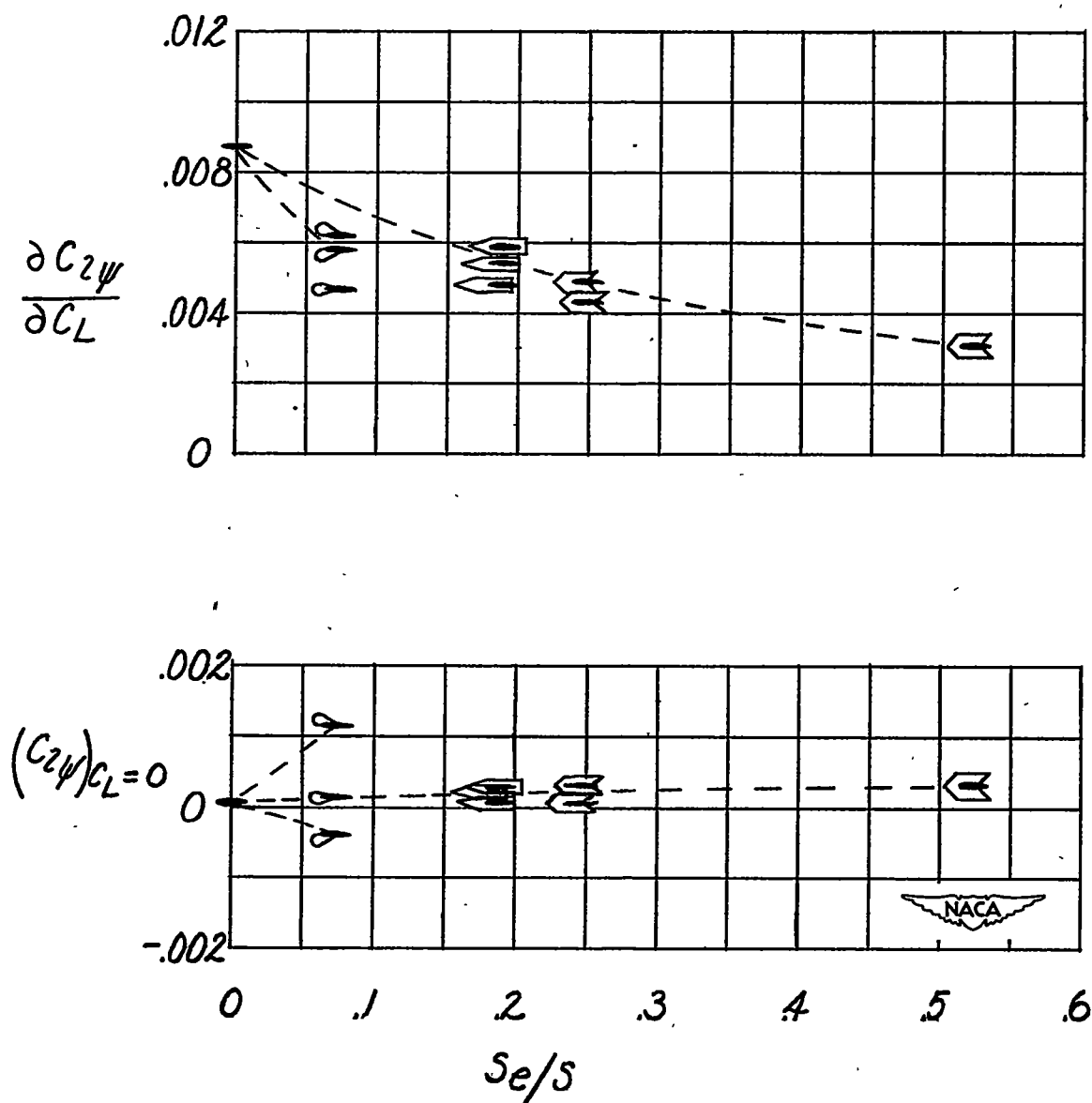
Figure 20.- Lateral-stability parameters $\left(C_{l\psi}\right)_{C_L=0}$ and $\partial C_{l\psi}/\partial C_L$ of the 46.7° sweptback wing of aspect ratio 4 with various end plates.
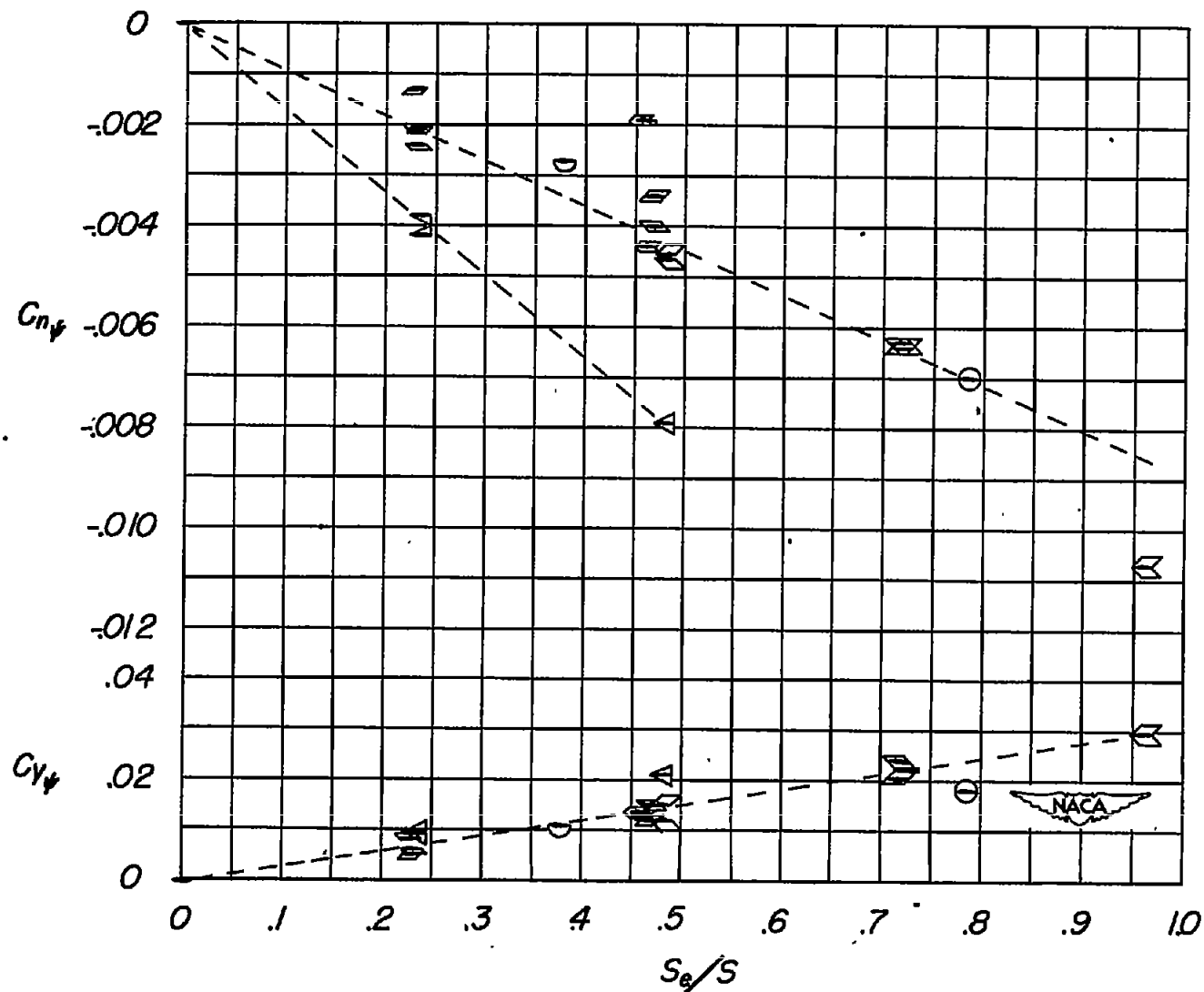
Figure 21.- Lateral-stability parameters C_{n_ψ} and C_{Y_ψ} of the 45° swept-back wing of aspect ratio 2 with various end plates. $C_L = 0.5$.
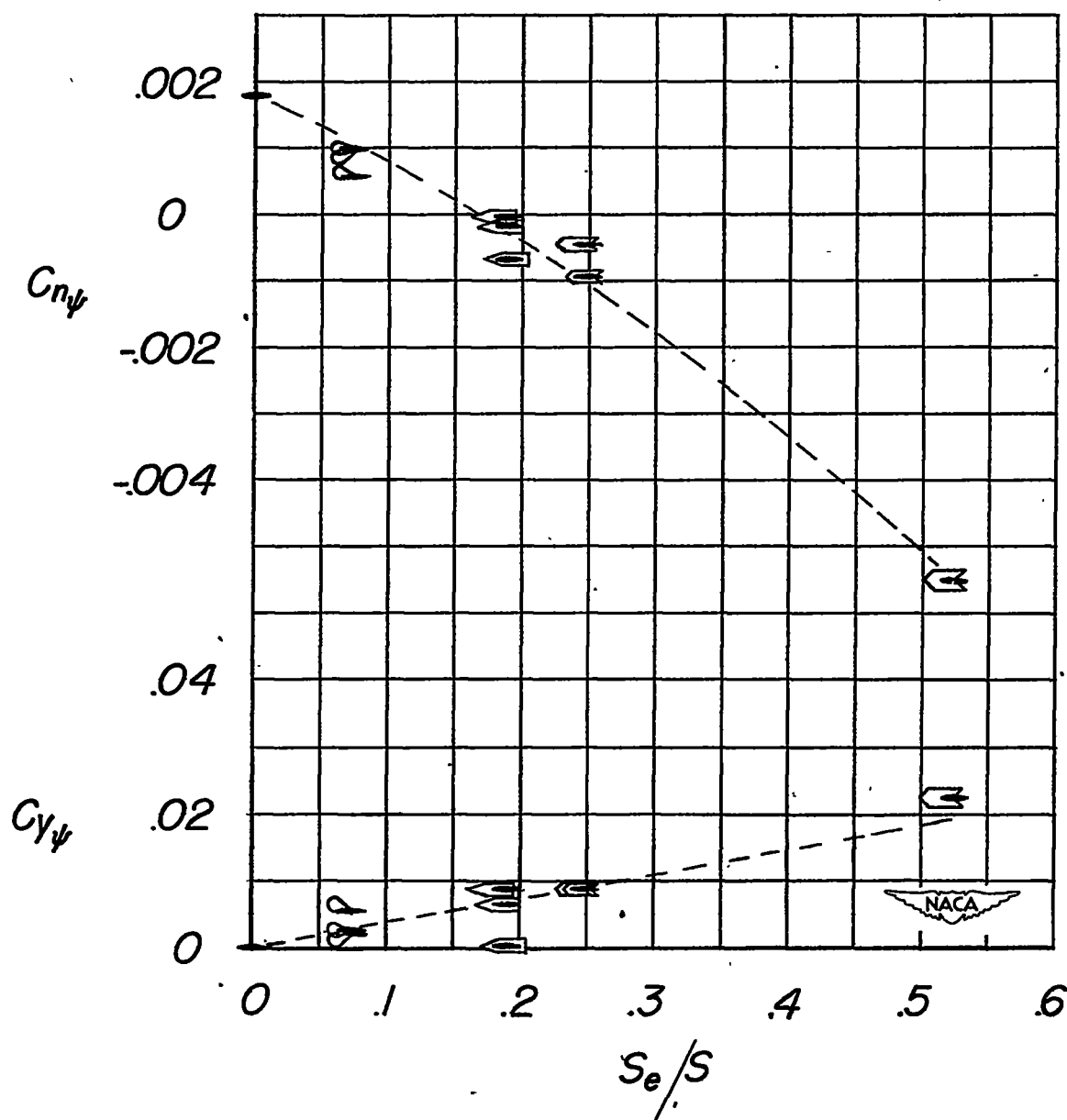
Figure 22.- Lateral-stability parameters C_{n_ψ} and C_{Y_ψ} of the 46.7° swept-back wing of aspect ratio 4 with various end plates. $C_L = 0.5$.
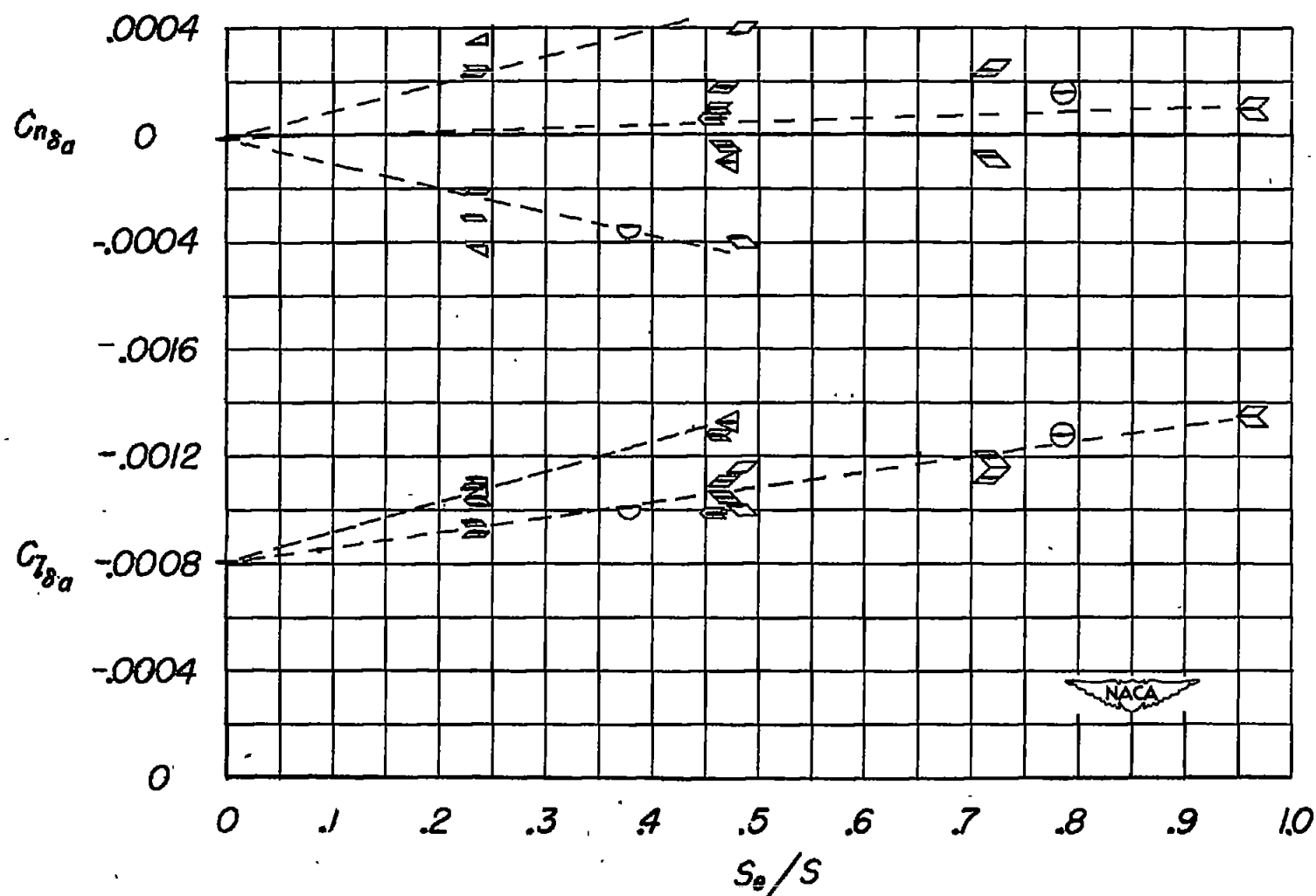
Figure 23.- Parameters $C_{n_{\delta_a}}$ and $C_{l_{\delta_a}}$ of the $45°$ sweptback wing of aspect ratio 2 with flap-type ailerons and with various end plates. $\alpha = 0°$.
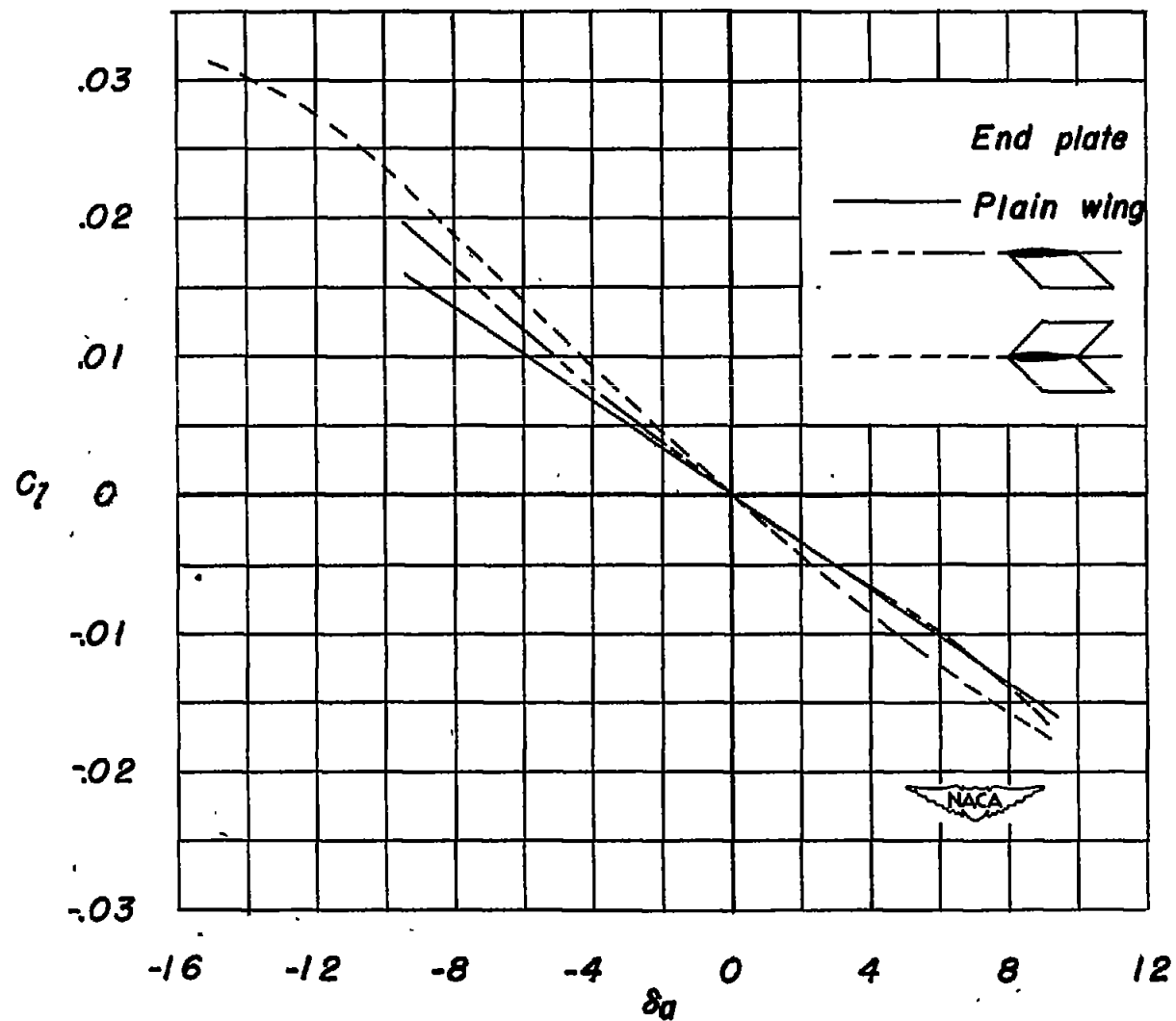
Figure 24.- Effect of two end-plate configurations on C_l resulting from aileron deflection on the 35° sweptback wing of aspect ratio 3. $\alpha= 6.5^\circ$.
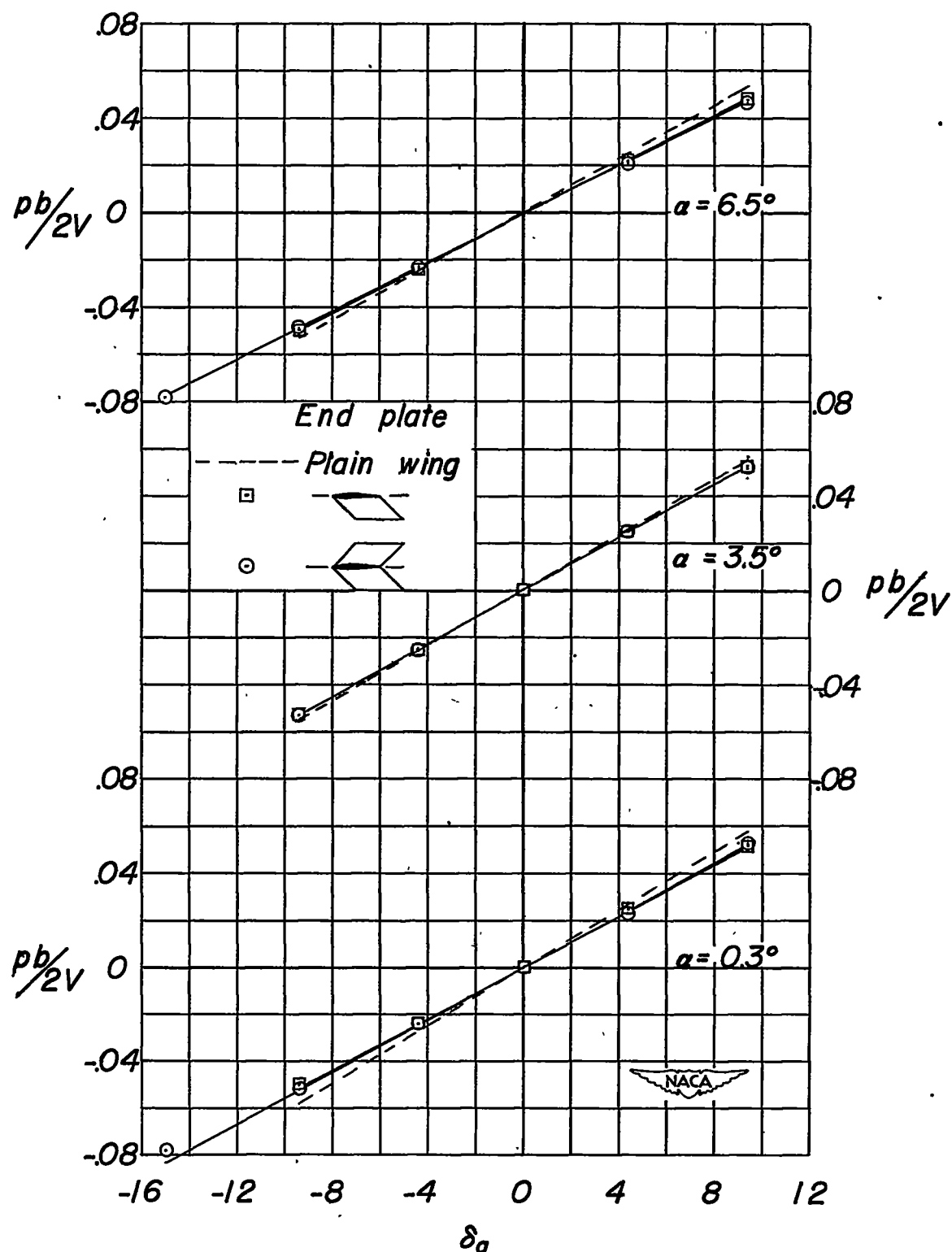
Figure 25.- Effect of two end-plate configurations on the variation of pb/2V with aileron deflection of the 35° sweptback wing of aspect ratio 3.
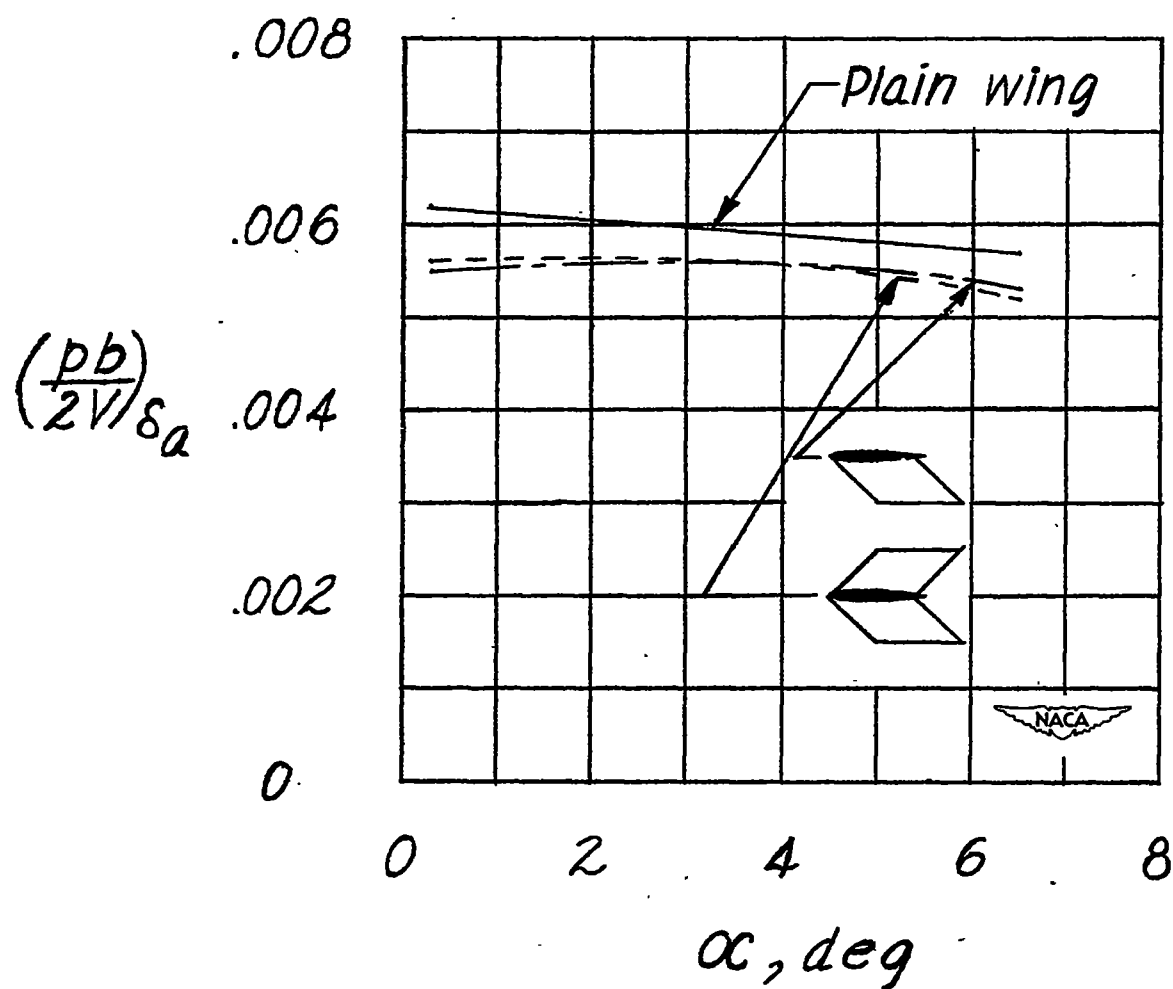
Figure 26.- Effect of two end-plate configurations on $(pb/2V)_{\delta_a}$ of the 35° sweptback wing of aspect ratio 3 in the low angle-of-attack range.